

**TRIBOLOGICAL BEHAVIOR OF
BORON MODIFIED AS CAST Ti-6Al-4V
ALLOYS**

M.Tech. Thesis

By
TULIKA DIXIT



**DISCIPLINE OF METALLURGICAL
ENGINEERING AND MATERIAL SCIENCE
INDIAN INSTITUTE OF TECHNOLOGY
INDORE**

JULY 2018

**TRIBOLOGICAL BEHAVIOR OF
BORON MODIFIED AS CAST Ti-6Al-4V
ALLOYS**

A THESIS

*Submitted in partial fulfillment of the
requirements for the award of the degree*

of

Master of Technology

by

TULIKA DIXIT



**DISCIPLINE OF METALLURGICAL
ENGINEERING AND MATERIAL SCIENCE
INDIAN INSTITUTE OF TECHNOLOGY
INDORE**

JULY 2018



INDIAN INSTITUTE OF TECHNOLOGY INDORE

CANDIDATE'S DECLARATION

I hereby certify that the work which is being presented in the thesis entitled **Tribological behavior of Boron modified Ti-6Al-4V alloys** in the partial fulfillment of the requirements for the award of the degree of **Master Of Technology** and submitted in the discipline of **Metallurgical engineering and Material science, Indian Institute of Technology Indore**, is an authentic record of my own work carried out during the time period from July 2016 to July 2018 under the supervision of Dr. K. Eswara Prasad, Assistant Professor, Department of Metallurgical Engineering and Material Science, Indian Institute of Technology Indore.

The matter presented in this thesis has not been submitted by me for the award of any other degree of this or any other institute.

Signature of the student with date

(TULIKA DIXIT)

This is to certify that the above statement made by the candidate is correct to the best of my/our knowledge.

Signature of the Supervisor of

M.Tech. thesis

(Dr. K. Eswara Prasad)

TULIKA DIXIT has successfully given his/her M.Tech. Oral Examination held on 06/07/2018.

Signature of Supervisor of M.Tech. thesis

Date:

Convener, DPGC

Date:

Signature of PSPC Member #1

Date:

Signature of PSPC Member #2

Date:

ACKNOWLEDGEMENTS

It is a pleasure to thank many people who made this work possible.

First and foremost, I would like to thank my advisor, Dr. K. Eswara Prasad whose support and guidance has driven me to do this work. His friendly nature gave me the freedom and opportunity to interact with him as much as I wanted to. He is one of the best teachers I have come across in my life.

I would like to take this opportunity to thank my PSPC members Dr. S.S. Hosmani and Dr. Devendra Deshmukh for their valuable time in assessing my work during the mid-term and end-term presentations and giving me valuable suggestions related to my work.

I am thankful to Dr. I.A. Palani, Head of the Department- MEMS for providing facilities that I required throughout the M Tech work. I am also thankful to the faculty of this Department for their support and effort in teaching the concepts in Materials Engineering.

I would like to express our thanks to Prof. U. Ramamurty (IISc) for lending the material used in this work. Profs. Palash Roy Chaudhary(MEC, Hyderabad) for allowing me to use wear testing machine facility, and Vamsi, Madhavan for helping me with Pin-on-Disc experiments.

I sincerely thank Dr. Satyajit Chatterjee for extending facilities of Tribology lab, Department of Mechanical engineering, IIT Indore for carrying out metallographic sample preparation and optical microscope characterization.

I thank Prof. N.K. Jain for extending Optical and Contact profilometer facilities of Metrology lab and wire EDM facility of Advanced manufacturing lab, Department of Mechanical engineering, IIT Indore.

I would also thank Sophisticated instrument center, IIT Indore for extending the SEM and XRD facilities and central workshop personnel for helping me with manufacturing stuff.

I express my gratitude to Lab supervisors and technicians Late Mr. Sachin Gayakwad, Mr. Mayur Dhake, Mr. Santosh Sharma, Mr. Suresh Bagore, Mr. Kinny Panday, Mr.

Nitin, Mr. Sandeep Gour, Mr. Deepak Rathore and Mr. Anand Pitare for helping me in carrying out the experiments.

I thank all my colleagues - Sheetal, Priyanka, Milind, Garima, Digvijay and Aditya for helping me out with experiments and materials. I also thank Shivam and Yeshwant for helping me in writing the thesis.

I thank my classmates and friends at the Institute for the good time I had here.

Finally, I thank my parents for their constant support.

DEDICATION

I dedicate my work to my parents for their selfless love and my Gurudev Sri Sri Ravi Shankar who brought me to the path which I always wanted to travel.

Synopsis

Trace additions of Boron to the Ti-6Al-4V melt leads to a substantial reduction in grain size by an order of magnitude, which in turn, minimizes or completely eliminates $\beta/\alpha+\beta$ working steps. This has a mixed effect on mechanical properties such as strength, fracture toughness, notch sensitivity, fatigue and creep performance. During the service, the components made of these alloys meet foreign objects and harder surface experiencing contact loading conditions. Hence it is important to understand the tribological behavior of these materials at both at room and elevated temperatures. Wear experiments were performed on Ti-6Al-4V samples having a different weight percentage of B (0, 0.3 and 0.55%), using Pin-on-disc tribometer at varying loads and temperature (from room temperature upto 573K) combinations. On carrying out wear experiments with the hard surface a nonlinear variation in the wear rate with respect to test temperature for all compositions of B modifies Ti-6Al-4V was observed. Ti64 having 0.3 wt.% B showed better wear properties especially at high temperature (573K) and higher loads as compared to 0.55 and 0.0 wt.% B. Wear experiment results shows severe wear at high temperature and for high B content (0.55B). To characterize wear tracks Scanning electron microscopy (SEM), profilometry, X-Ray diffraction (XRD) and subsurface optical microscopy is used. Characterization results clearly show prominent delamination wear at high temperature especially for 0.55B and for low temperature and low B content more adhesive wear is reported.

LIST OF PUBLICATIONS

- This work was presented in international conference NMD ATM 2017 organized by The Indian Institute of Metals (IIM) at the BITS Pilani- KK Birla, Goa campus from 11th to 14th November 2017.
- This work is submitted to Wear journal with the title “Room and high temperature wear behavior of Boron modified as-cast Ti-6Al-4V alloys against hardened steels”

TABLE OF CONTENTS

1	Introduction.....	1
1.1	Crystal structures of Ti and the role of alloying elements	1
1.2	Deformation modes in Titanium	1
1.3	Features of Ti-6Al-4V alloys	2
1.4	Solidification and thermomechanical processing of Ti alloys	2
1.5	Effect of B addition in Ti64 alloys.....	3
1.6	Importance of Tribological study of B modified Ti64 alloy.....	3
2	Literature review	8
3	Methodology	13
3.1	Materials.....	13
3.2	Sample machining for microstructural characterization and wear experiments	13
3.3	Microstructural characterization of machined samples.....	14
3.3.1	Sample polishing.....	14
3.3.2	Microstructural Characterization using Scanning electron microscope (SEM)	14
3.4	Wear test experiments	15
3.5	Wear track characterization.....	16
3.5.1	Characterization of samples using SEM	16
3.5.2	Profilometry analysis of the worn surfaces.....	16
3.5.3	Characterization through XRD (X-ray diffraction)	16
3.6	Subsurface microstructure characterization using an optical microscope	17
4	Results.....	19
4.1	Microstructure	19
4.2	Pin on disc wear test.....	19

4.3	SEM analysis of wear morphology	20
4.4	Profilometer analysis of wear tracks	21
4.5	XRD analysis of wear tracks	21
4.6	Subsurface microstructure analysis:.....	21
5	Discussion.....	30
5.1	Analysis of results of the pin on disc experiments.....	30
5.2	Morphologies of the worn-out surfaces	35
5.3	Subsurface microstructures	36
5.4	Formation of surface oxides and their influence on the wear behavior	37
6	Conclusion and future scope.....	39

LIST OF FIGURES

Figure 1.1 Classification of engineering metals based on the density and unique properties of Titanium[5].	4
Figure 1.2 Applications of Ti alloys a) bioimplants [6] b) aerospace jet engine[1].	4
Figure 1.3 Allotropic forms of Ti (a) HCP below 882 °C and (b) BCC above 882 °C along with the close packed planes[1].	5
Figure 1.4 Phase diagram of Ti alloys indicating the role of alloying elements on stabilization of α and β phases[1].	5
Figure 1.5 Bubble chart comparing the specific strength of Ti-Al alloys with other structural materials [7].	6
Figure 1.6 Lamellar $\alpha+\beta$ microstructure of Ti-6Al-4V alloy observed under (a) Optical microscope and b) Transmission electron microscope (TEM).	6
Figure 1.7 a) Typical thermomechanical processing cycle of a Ti64 alloy[1] and the corresponding end microstructure processed using (b) route 1 and (c) route 2[2].	7
Figure 1.8 Representative microstructures of Boron modified Ti64 alloys with (a) 0.0B (b) 0.09B and (c) 0.55B the gray background is α , white is β and dark is TiB [8].	7
Figure 2.1 The role of Boron on mechanical properties of as-cast Ti64 alloys showing the variation of (a) grain and lath sizes b) ultimate tensile strength and ductility c) elastic modulus and yield strength d) mode I fracture toughness, with B content [11].	11
Figure 2.2 Variation of fatigue strength with B content in Ti64-B alloys.[13].	12
Figure 2.3 Scanning electron micrographs indicating the interaction between the slip traces and laths at different plastic strain for a) 0 wt% B and b) 0.09 wt% B.[15].	12
Figure 3.1 Specimens used for hardness and wear experiments (a) Cube of edge length 3mm (b) cylindrical pins of diameter 8mm and length of 20 mm.	17

Figure 3.2 Schematic representing the working principle of wire EDM[21].....	17
Figure 3.3 Macroscopic image of the hot mounting specimen used for metallographic examination.....	18
Figure 3.4 Schematic representing the working principle of pin on disc tribometer...	18
Figure 3.5 (a) Macroscopic optical images of the wear surface of cylindrical pin (b) Sample section for sub-surface microstructural examination (c) mounting of sectioned surface.....	18
Figure 4.1 Scanning electron microscopy images of microstructures of Boron modified Ti64 alloys with (a) 0.0B (b) 0.3B and (c) 0.55B.....	22
Figure 4.2 Variation of wear, w with time, t obtained from Pin-on-disc tribometer...	23
Figure 4.3 COF plotted against the sliding distance at a normal load of 25N.....	23
Figure 4.4 Variation of wear rate, η with temperature at 25N load for the three different Ti64-B alloys.....	24
Figure 4.5 Variation of wear rate η with Boron content at 25N load at different temperatures.....	24
Figure 4.6 Representative plot showing the variation of COF with temperature at a constant load of 25N for all three alloys.....	25
Figure 4.7 SEM images of wear surfaces of Ti64 alloys tested at 25N under various combinations of temperature and composition of (a) 300 K, 0 B (b) 573 K, 0 B (c) 300 K, 0.3 B (d) 573 K, 0.3 B(e) 300 K, 0.55 B (f) 573 K, 0.55 B.....	26
Figure 4.8 Contact profilometer images of the worn-out surfaces of Ti64 alloys tested at 25 N for composition and temperature of (a) 0B, 300 K (b) 0 B, 573 K (c) 0.3B, 300 K, (d) 0.3 B, 573 K (e) 0.55 B, 373 K (f) 0.55 B, 573 K.....	27
Figure 4.9 XRD patterns obtained on the wear surfaces of Ti64-B samples subjected to wear testing at (a) 300 K and (b)573 K.....	28

Figure 4.10 Cross sectional optical micrographs of sub-surface regions just below the wear surface of Ti64 alloys tested at 25 N under (a) 0B, 300 K (b) 0 B, 573 K (c) 0.3B, 300 K, (d) 0.3 B, 573 K (e) 0.55 B, 300 K (f) 0.55 B, 573 K.....29

Figure 5.1 Prominent types of wear mechanisms [24].....32

LIST OF TABLES

Table 5-1 Table explaining the effect of B on properties and factors/ properties that govern wear rate and COF.....33

1 Introduction

Titanium and its alloys have widespread applications in the lightweight structural applications because of their high specific strength (almost comparable to superalloys), elevated temperature mechanical properties, good corrosion resistance (even for saline water), bio-compatibility and non-magnetic properties. These properties make them suitable candidates for aerospace applications, chemical processing plants, biomedical applications[1] as shown in Figure 1.1 and Figure 1.2

1.1 Crystal structures of Ti and the role of alloying elements

At room temperature, Ti exhibits a hexagonal close-packed (HCP) crystal structure and upon heating, it undergoes an allotropic transformation from HCP α phase to body-centered cubic (BCC) β phase above 882°C as shown in Figure 1.3. α phase of Ti has HCP crystal structure which has very few slip system making it more brittle. Ti is highly reactive to Oxygen and Hydrogen causing its embrittlement at a higher temperature, therefore, Ti cannot be used in pure form for most applications. Alloying Ti with other elements improves its properties. The transformation temperature, T_{tr} , is affected by the addition of interstitial and substitutional alloying elements. The alloying elements such as Aluminium, Oxygen, Nitrogen, Carbon, Boron stabilizes the α -phase by increasing the T_{tr} above 882°C and hence are known as α -stabilizers while elements such as Vanadium, Molybdenum, Niobium increases the stability of the β phase by reducing the T_{tr} . Few elements like Zr and Hf stabilizes both α and β phases and hence are referred to as neutral stabilizers. At low concentrations, these stabilize the α -phase while at high concentrations they stabilize β phase (Figure 1.4)

1.2 Deformation modes in Titanium

The most commonly observed slip system in α -Ti are planes are basal (0001), prismatic $\{101\bar{0}\}$ and pyramidal $\{101\bar{1}\}$ planes along with the closest packed $\langle 112\bar{0} \rangle$ direction. The lattice parameter ratio (c/a) ratio of 1.587, which is 6% lower than ideal c/a ratio of a HCP lattice, because of which the slip occurs on prismatic planes in contrast to the basal planes. At room temperature, HCP-Ti does not contain minimum 5 independent slip systems needed for homogeneous plastic deformation by slip alone, therefore twinning plays a prominent role in the plastic deformation. Unlike α -

Ti, β -Ti having BCC crystal structure has a large number of slip systems and hence exhibits better plasticity. The active slip systems for this phase are the closest packed $\{110\}$ plane along with most densely packed $\langle 111 \rangle$ direction.

1.3 Features of Ti-6Al-4V alloys

Of all the Ti alloys, the Ti-6Al-4V (hereafter referred as Ti64) an $\alpha+\beta$ titanium alloy containing 6% Al and 4% V is most widely used for industrial applications due to its enhanced mechanical properties compared to the other Ti alloys. $\alpha+\beta$ alloys contain both α and β phases (15% β phase) at room temperature and have cumulative properties of both the phases such as good ductility, room and elevated temperature strength, fatigue and fracture resistance. Figure 1.5 shows a comparative chart of the specific strength of Ti64 with other alloys. The enhanced properties are attributed to the lamellar microstructure which is typically obtained by following a specific heat treatment procedure highlighting the importance of heat treatment of these alloys. In Ti64 alloys, the major role of V is β stabilizer while Al is increasing ductility. The as-cast microstructure of Ti64 alloys comprises of very coarse grain size with inferior mechanical properties making them unsuitable for most engineering applications. Therefore, all the cast Ti64 alloys are subjected to elevated thermomechanical processing to refine the microstructure followed by a series of heat treatment steps. A typical wrought processing and heat treatment cycle of a Ti64 alloy is shown in Figure 1.7.

1.4 Solidification and thermomechanical processing of Ti alloys

When $\alpha + \beta$ Ti is cooled from high temperature, α phase starts nucleating at the grain boundaries of β phase, on further cooling α platelets nucleate at these α laths which are formed along β grain boundaries. According to Burger's orientation relationship these α colonies grow until they meet other colonies. Within the colonies, α plates are separated from each other by a retained β matrix which is also called β lath. This microstructure appears as lamellar, where the thickness of α lath is more than β laths. When cooling rate (from β phase) increases, the nucleation starts not only at the grain boundaries but also at the colonies itself (a non homogeneous type of nucleation), these other α laths grow perpendicular to laths growing at grain boundaries forming a basket weave structure also known as a Widmanstatten structure. (Figure 1.6)

Processing route for Ti64 alloys is shown in Figure 1.7. After homogenization of cast Ti64 deformation processing (step II) which can be rolling, forging etc. can be done by heating in either of the two phases, $\alpha + \beta$ or β . Since β phase has better ductility and thermal properties, it is preferable to carry out step II in this phase. Also, the resulting microstructure obtained by this β processing is lamellar (alternating α/β laths) and has better mechanical properties. If the processing in step II is carried out in the $\alpha + \beta$ phase then microstructure has equiaxed α with fine acicular α and β . This microstructure does not possess good mechanical properties and therefore for high strength applications, it is always preferable to carry out processing in the β phase[2]. Step III is recrystallization followed by annealing in step IV. The rate of annealing decides the thickness of α laths, colony size etc. In the above-mentioned steps a lot of energy is consumed in maintaining high temperature (200-300° above β transus) for carrying out deformation processing, therefore this makes β processing non economical and alloy more expensive.

1.5 Effect of B addition in Ti64 alloys

Zhu *et al.*[3] first reported the grain refinement in of Commercially Pure (CP) Titanium by elemental Boron addition, then further work on Boron addition in Ti64 is reported by Tamiriskandala *et al.*[4] which states that cast grain size is reduced by an order on B addition in Ti64 alloys thus eliminating the expensive hot-working step. The solubility of B is very low in Ti thus B precipitates in the form of TiB whiskers. These whiskers are elongated needle-shaped with an aspect ratio of 8-9 and have an orthogonal crystal structure. The TiB particles preferably orient themselves on the prior β grain boundaries and when their concentration increases they form necklace like structure around grain boundaries as shown in Figure 1.8.

1.6 Importance of Tribological study of B modified Ti64 alloy

Significant work has been done to study the mechanical behavior of B modified Ti64 alloys like fatigue, fracture toughness, creep behavior, elastic and plastic properties etc. by Sen and co-workers. During the service, the components made of these alloys meet foreign objects experiencing contact loading conditions. For example, jet engines used in the aerospace application have piston and cylinder arrangement and other mating parts as well which are under surface contact condition. Another example is the disc brakes that are used in aircraft are under extreme contact loading

conditions. Hence it is important to understand the tribological behavior of these materials at both room and elevated temperatures.

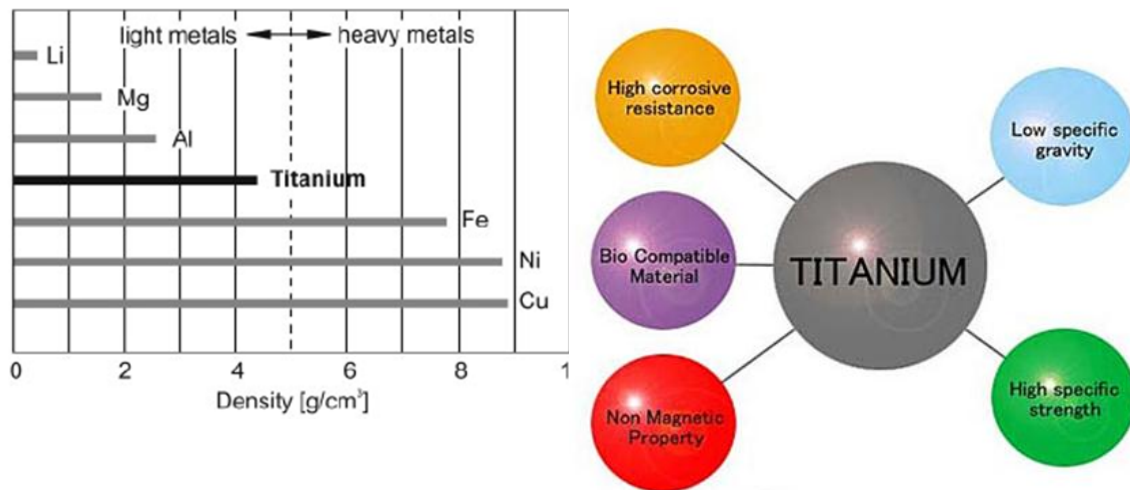


Figure 1.1 Classification of engineering metals based on the density and unique properties of Titanium[5]

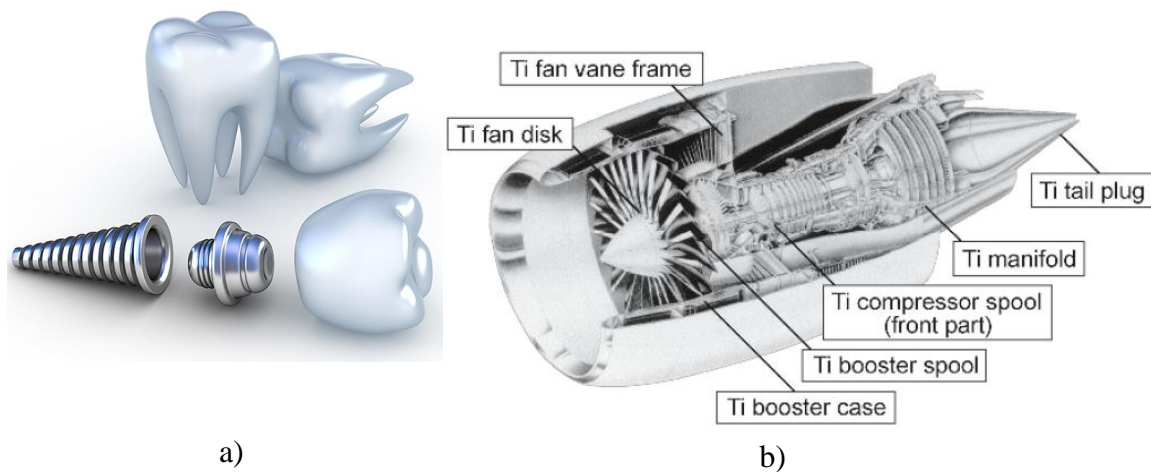


Figure 1.2 Applications of Ti alloys a) bioimplants [6] b) aerospace jet engine[1]

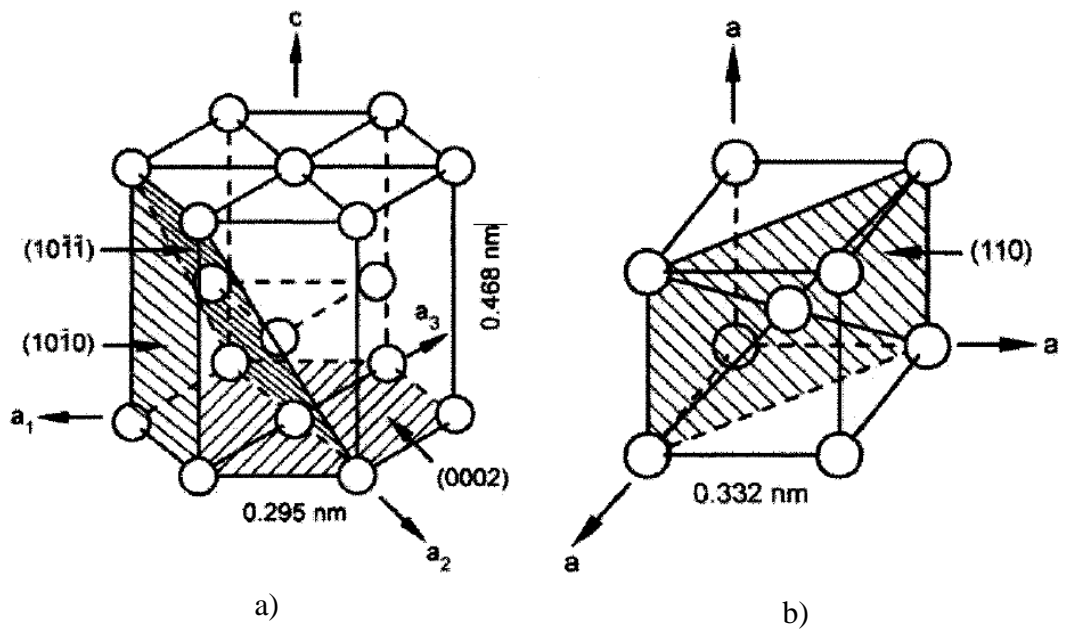


Figure 1.3 Allotropic forms of Ti (a) HCP below 882 °C and (b) BCC above 882 °C along with the close packed planes[1]

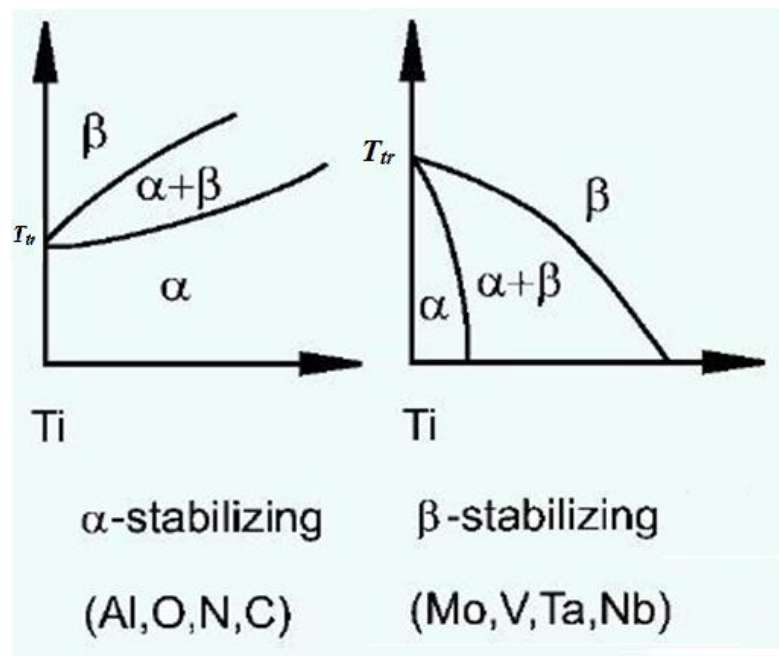


Figure 1.4 Phase diagram of Ti alloys indicating the role of alloying elements on stabilization of α and β phases[1]

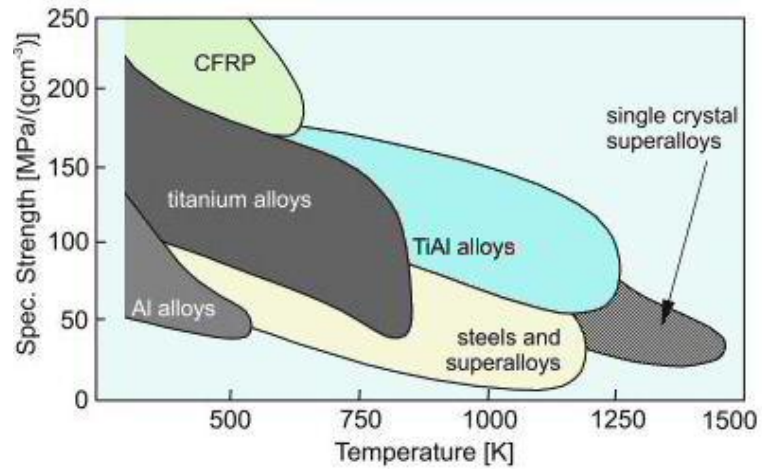


Figure 1.5 Bubble chart comparing the specific strength of Ti-Al alloys with other structural materials [7]

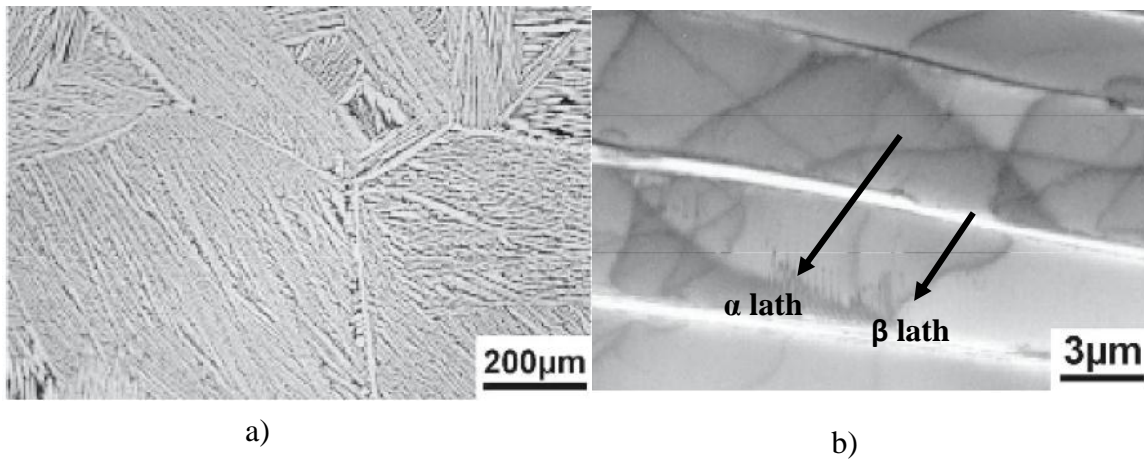


Figure 1.6 Lamellar $\alpha+\beta$ microstructure of Ti-6Al-4V alloy observed under (a)Optical microscope and b) Transmission electron microscope (TEM)

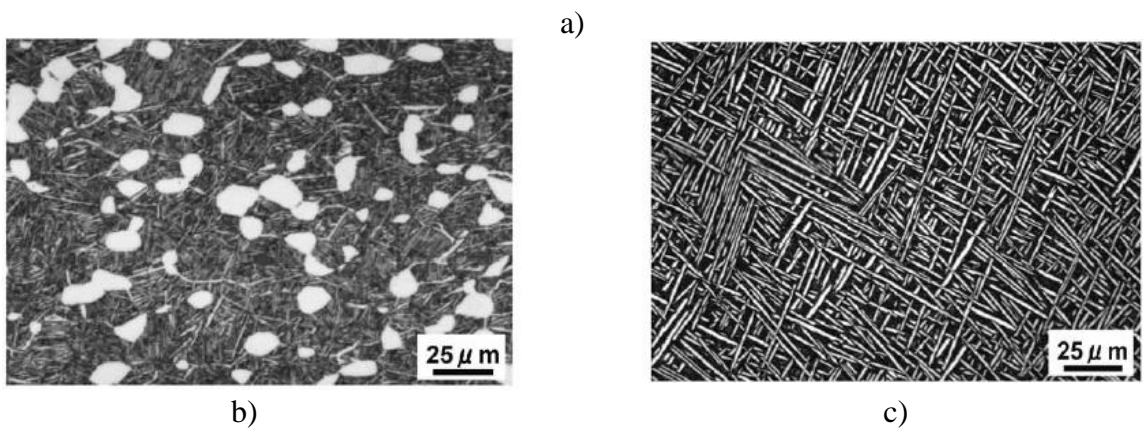
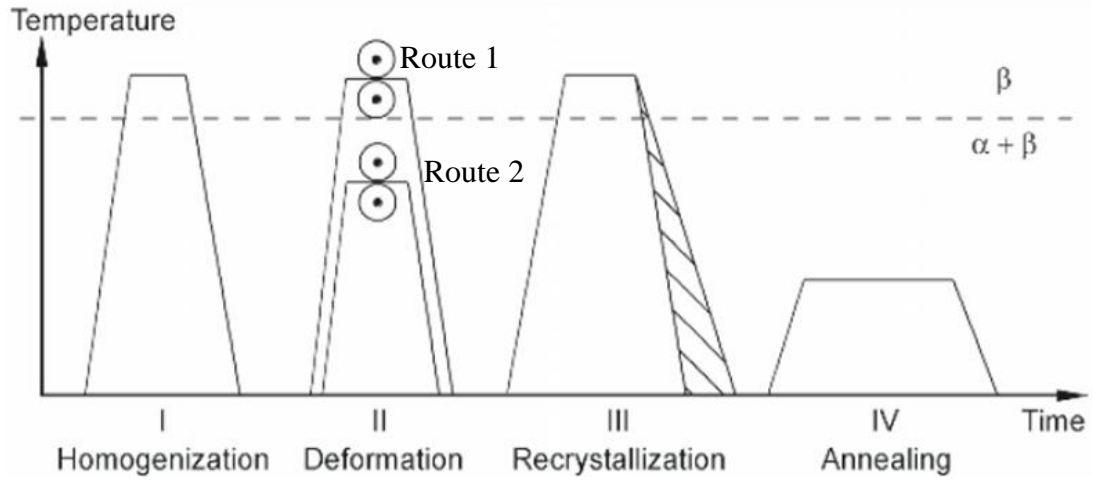


Figure 1.7a) Typical thermomechanical processing cycle of a Ti64 alloy[1] and the corresponding end microstructure processed using (b) route 1 and (c) route 2[2]

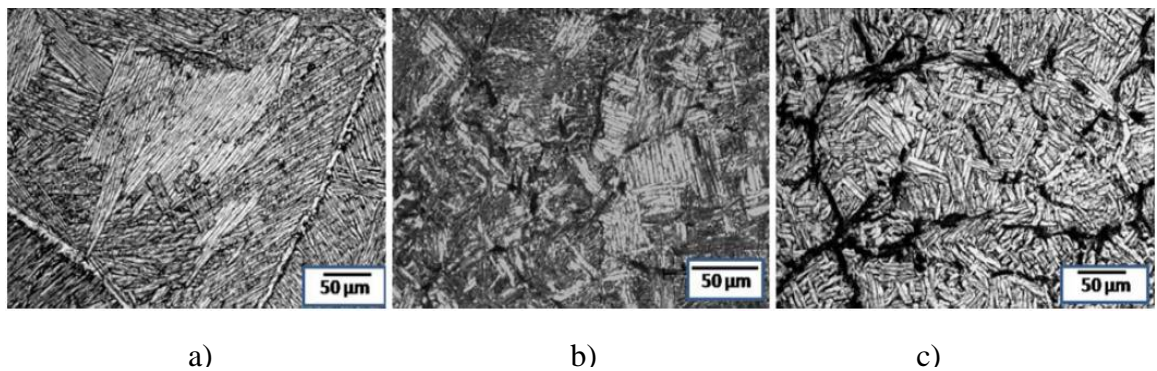


Figure 1.8 Representative microstructures of Boron modified Ti64 alloys with (a) 0.0B (b) 0.09B and (c) 0.55B the gray background is α , white is β and dark is TiB [8]

2 Literature review

A large number of studies have been performed on the mechanical properties of wrought Ti64 alloys. Since the focus of the current study is on Boron modified cast Ti64 alloys, we review the literature pertaining to experimental investigations performed on the mechanical properties of as-cast Ti64-B alloys.

Zhu *et al.*[3] reported that elemental addition of Boron to the commercially pure Ti resulted in a substantial increase in strength and ductility up to 0.09 wt.% B addition. Further additions of B caused a reduction in ductility while the strength continues to increase. The increase in mechanical properties is attributed to the microstructural changes taking place due to the addition of Boron. They observed substantial grain refinement which leads to the enhancement of both strength and ductility while the TiB precipitate network at the grain boundaries is responsible for the loss of ductility. This could be due to weak TiB-matrix interface. Further, the precise role of Boron on the microstructure was discussed in detail in a review article by Tamiriskandala and Miracle [4] with a reference to Ti-B phase diagram. According to the Ti-B binary phase diagram, the maximum solubility of B is less than 0.02 % at room temperature under equilibrium conditions. So the excess B chemically reacts to form an intermetallic compound TiB (although the exact stoichiometry is still unknown) which are typically needle shape. These precipitates form a necklace type of network along the prior β grain boundaries as shown in Figure 1.8. Being an intermetallic compound TiB has a higher melting point and strength compared to the matrix but and have a comparable density (4.56 g/cm^3) and coefficient of thermal expansion ($6.2 \times 10^{-6}/\text{K}$ for TiB and $8.6 \times 10^{-6}/\text{K}$ for Ti64 at room temperature) [9][10]. In the hypoeutectic region, the primary β is formed prior to the formation of TiB particles ruling out the proposition of TiB particle-assisted grain refinement. Rather the reason for grain refinement is due to the constitutional super-cooling promoted by the elemental B which causes a solute partitioning at the solidification front. While the grain refinement is caused due to the addition of elemental B, TiB particles (present at the prior β grain boundaries) restrict the grain growth at a higher temperature by Zener pinning mechanisms effect. According to this, the presence of small and hard particles in polycrystalline alloys creates a pinning pressure on the movement of high and low angle grain boundaries and thus preventing the grain growth even at a high

temperature. $\beta \rightarrow \alpha$ transformation mechanics is influenced by TiB providing additional nucleation sites for α laths, therefore, the size of α lath reduces as TiB concentration increases. It was reported in this study that trace addition of B in as-cast Ti64 alloys increase the strength and stiffness to 20%. They also summarized various processing routes of Boron modified Ti alloys like boron addition in the cast, pre-alloyed and blended elemental technique.

Sen *et al.*[11] studied microstructural effects on some mechanical properties like elastic modulus, yield strength, ultimate tensile strength and fracture toughness of B modified Ti64 alloys. The common feature for all the alloys having a different weight percentage of B was that they show elastic-perfectly plastic behavior having strain hardening constant $n \approx 0.08$. On adding just 0.1 wt % B there was almost 91% reduction in grain size (d), approximately 40% in α lath size (λ), increase of 8.4% in Young's modulus (E), almost 7% in yield (σ_y) and ultimate tensile strength (σ_u), 14% increase in Vicker's hardness value and approximately 48% reduction in fracture toughness (K_{Ic}). All these results are summarized in Figure 2.1. Improved yield strength is attributed to Hall Petch mechanism, according to this, the grain boundaries act as an obstacle for dislocation motion. This depends on the orientation of the grains, as slip planes do not match, dislocation cannot slide through them since they have to change their direction, and therefore there is a large amount of dislocation pile up. Finer the microstructure more will be the grain boundaries and more hindrance to dislocation motion. Improvement in strength can also be credited to load sharing mechanism of TiB particles. The reason behind the decrease in fracture toughness due to addition of Boron is the pointed tips of TiB whiskers that act as a region of stress concentration. When the cracks propagate the plastic region ahead of the crack tip gets easily fractured due to the high-stress concentration. Another reason can be explained by the RKR (Rice Knott Richie) model, according to this model for a crack to propagate across the laths the maximum principal stress should exceed the maximum tensile/fracture stress at a critical distance. This critical distance is in the order of few α lath sizes and as the α lath size decreases the critical distance decreases, therefore, the fracture toughness decreases[12].

Sen *et al.* [13] also studied the fatigue behavior of these alloys. They reported that fatigue strength improved on B addition (Figure 2.2) and there is cyclic softening which increases linearly on B addition (except at a concentration of 0.04 wt % B). The

strain incompatibility between stiffer TiB particles and the remaining matrix produces dislocations. The movement of dislocations across β laths is difficult due to incompatibility between two phases so they accumulate at α/β boundary. As the dislocation pile-up increases, the slip phenomenon gets triggered in other α laths that might have favorable orientation. This generates plastic flow and cyclic softening. Fatigue strength of Ti64 alloys directly depends on α lath size, lesser the size more is the dislocation pile up.

Another study by Sen and Ramamurthy [14] shows that the variation of volume percentage of TiB particles is linear with respect to percentage boron in the Ti64 alloy, this suggests almost all the boron gets precipitated out in the form of TiB particles. They carried out nanoindentation experiments to find average elasticity modulus (E) of B- Ti64 by finding out E for α , β , and TiB particles. Value of E for α is higher than β due to close packing of HCP crystal structure. Value of E for TiB particles is highest because of their stiffness and also standard deviation in E values is more than others due to high anisotropy. The cumulative result is that the value of E for B- modified Ti64 alloys increase with B content.

Agrawal and Karthikeyan [15] reported the strain hardening phenomenon in these alloys. They stated that the grain colony boundaries are more responsible for strengthening and strain to harden since slip transmission is not as easy as lath boundaries, this is due to the difference in lattice matching between two colonies. Therefore more the dislocation pile up more is the strain hardening. As these colony boundaries resist slip transfer they also promote multiple slips. Therefore higher the boron content, finer the grain size i.e., more is the grain boundary which results in multiple slips. In multiple slips, the secondary slips get activated which homogenizes deformation. As shown in Figure 2.3 the alloy having no B shows only one slip line.

G. Singh *et al.*[16] compared tensile and fatigue properties of B modified Ti64 alloys for as cast and as forged condition. They found that at high-temperature tensile strength and stiffness also improves on B addition. They also reported that B Addition is beneficial for creep properties due to an increase in the number of interfaces which will mitigate the dislocation mobility and thus decrease the steady-state creep rate[17].

Another study has been done on the combination of high temperature (in $\alpha+\beta$ range) and strain rate effects. It has been reported that at high temperature and low strain rate, flow softening is observed due to dynamic globulisation. At high strain rate, oscillations are observed due to kinking of laths, breaking and bending of β boundaries and cracking of TiB particles leading to matrix cavitation [18].

The following theory and concepts behind these studies helped us further in understanding wear mechanisms and the effect of microstructure on them.

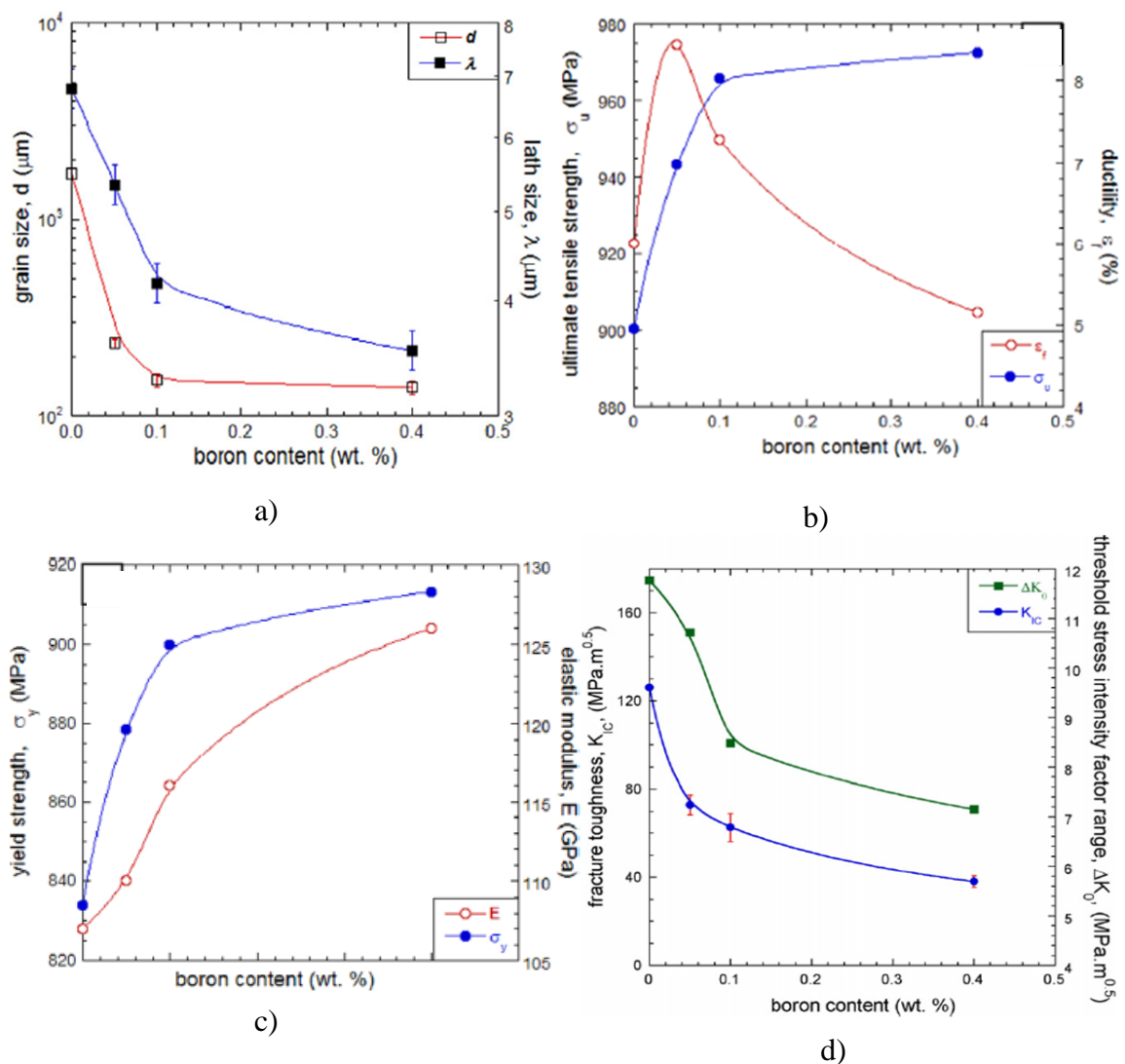


Figure 2.1 The role of Boron on mechanical properties of as-cast Ti64 alloys showing the variation of (a) grain and lath sizes b) ultimate tensile strength and ductility c) elastic modulus and yield strength d) mode I fracture toughness, with B content [11]

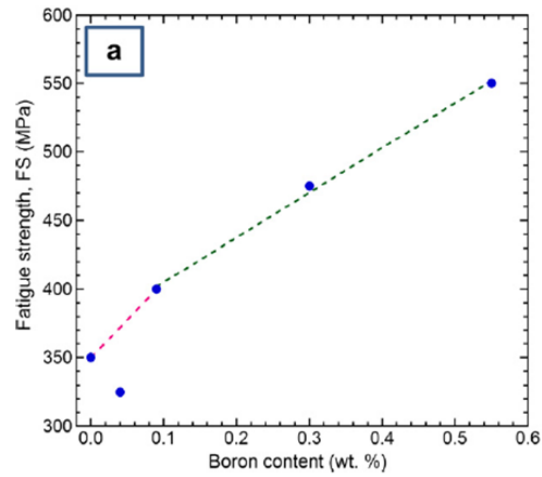


Figure 2.2 Variation of fatigue strength with B content in Ti64-B alloys.[13]

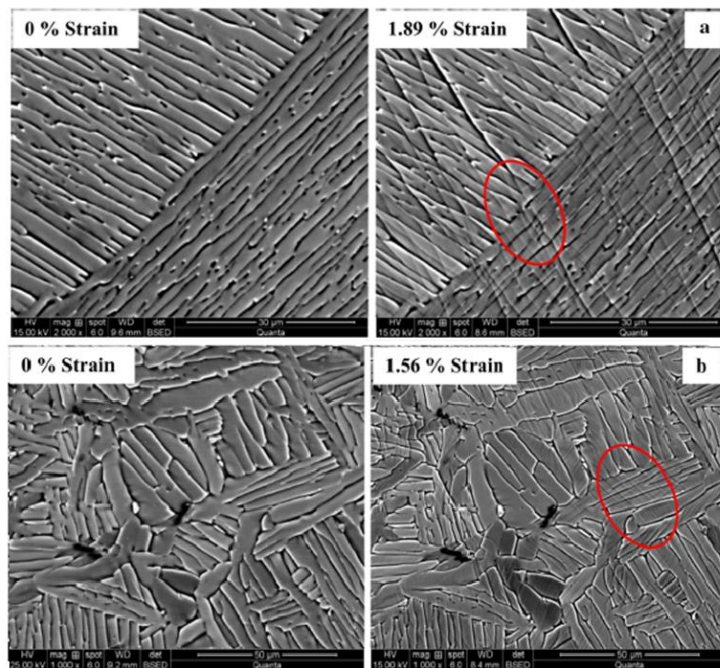


Figure 2.3 Scanning electron micrographs indicating the interaction between the slip traces and laths at different plastic strain for a) 0 wt% B and b) 0.09 wt% B.[15]

3 Methodology

This chapter deals with a detailed description of materials, sample preparation procedures, experimental methods, pre and post characterization techniques used for specimen analysis in the current work.

3.1 Materials

The cast ingots of Boron modified Ti64 alloys (having Boron content 0.3B and 0.55B) having a diameter of 75mm and length of 180mm are prepared at Flow serve corporation (Dayton, OH). The casting of Ti64 is done via induction skull melting (ISM) under a controlled atmosphere using an induction coil after which Boron is added in an elemental form which completely dissolves in the above melt. Hot isostatic pressing (HIP) is carried out for 2 hrs at a temperature of 1173K and pressure of 100MPa to ensure that the castings are devoid of porosity.

3.2 Sample machining for microstructural characterization and wear experiments

Samples for microstructural characterization and wear experiments are machined from cast ingots by wire - electric discharge machining (EDM). Cuboid samples of 3 mm in edge length are used for microstructural analysis (Figure 3.1a) while cylindrical samples with an 8mmdiameter and 20mm length (Figure 3.1 b) are used in wear experiments. Unlike conventional machining process, EDM provides good surface finish, less mechanical vibrations, less thermal damage, minimum residual stresses and there is less damage to the material surface due to heat production[18]. Specific heat conductivity of Ti is poor, which can produce thermal stresses in the material if it is being machined by conventional processes. Working of wire EDM takes place by spark erosion of metal when a large voltage is generated between the two electrodes (one is the brass wire and the other is a working electrode which is workpiece). The high voltage results in the breakdown of the dielectric fluid between electrodes causing current to freely flow from one electrode to another. As a result, a large amount of heat is generated at a very narrow region approximately 12000°C [18]causing the metal to melt/ vaporize away from that spot. The molten metal is flushed out by the dielectric fluid. The machine used in our experimental setup is numerically controlled where the brass wire and travels through the workpiece for material removal. The wire is continuously fed using a spool as it gets consumed up

while machining. The brass wire used in this experimental setup is zinc coated with the diameter of 0.25mm. The machining voltage and ignition pulse current are maintained at 80V and 6-18A respectively with the wire feed rate of 4m/s[19]. The basic working principle of wire EDM is shown in Figure 3.2

3.3 Microstructural characterization of machined samples

3.3.1 Sample polishing

Samples are hot mounted using SimpliMet3000 mounting press of Buehlermake. The Ti64-B samples are placed on the mounting mould completely covered with Pheno cure powder having phenolic thermosetting resin. Under the action of high temperature and pressure, the resin melts inside moulds and covers the specimen, subsequently on cooling the resin sets and becomes hard. The mounted samples as shown in Figure 3.3 are then polished using an EcoMet polishing machine of Buehler make. The samples are polished with emery papers with the starting grit size of 240, then on 320, 400, 600, 800, 1000, 1500, 2500 and 4000 for 10 minutes each. A steady supply of water is always maintained while polishing and the sample is also held in fixed position so that all the scratched are in one direction. When the next size grit size emery paper is taken for polishing the sample should be held in such a way that the direction of material removal is perpendicular to the direction of lay. Final polishing is done with 3 μ m diamond paste over the velvet cloth until mirror finish is obtained. The polished specimen is cleaned ultrasonically first with ethanol and then with distilled water for 5 minutes each and finally, air dried using the blower.

3.3.2 Microstructural Characterization using Scanning electron microscope (SEM)

After metallographic preparation, the microstructural examination was conducted by etching the surface of the sample with a suitable etchant. Etching preferentially oxidizes all the boundaries like grain, colony and lath boundaries, thus other matrix gets highlighted which can be clearly observed under optical or scanning electron microscope. The etchant used for Titanium alloys is Kroll's reagent having a composition of 2% HF, 6% HNO₃ and 92% distilled water by volume. Etching is done by swabbing the polished face of the specimen for about 10-15s using a cotton swab followed by washing it by tap water and drying the etched surface with a hot blower.

Field emission scanning electron microscope (FE-SEM) of Supra55 Zeiss make is used to observe microstructure. The basic working of SEM is the scanning of the specimen using a focused beam of electrons that are produced in an electron gun using the high electric field. Secondary electron scanning mode at 5KV electron beam is used to detect the microstructure. These secondary electrons that are generated from the sample due to striking off the surface electrons with the electron beam, gives an image with a good resolution of the topography of the sample. Since Titanium alloys are not a very good conductor of electricity the specimen is glued on a stub with a carbon tape and gold coating the surface.

3.4 Wear test experiments

Wear experiments are performed using pin-on-disc tribometer of DuCom make and the basic working principle of the machine is shown in Figure 3.4. In this test, the tribo wear of specimen which is in the form of stationary cylindrical pin happens against a rotating hardened disc. The disc is made of EN31 stainless steel having a diameter of 160mm and thickness of 8mm with the hardness of 60HRC. The experiments were performed by heating the pin at different temperatures (300K, 373K, 473K, and 573K) and varying load at each temperature starting from 5N up to 25N, increasing with steps of 5N. The disc was maintained at room temperature as well as constant rpm.

In order to maintain proper contact between the sliding surfaces, the pin surface is polished using emery paper till 2500 grit size. In the experiments, the disc rotation is set to 650rpm for 30 minutes and the stroke length of the pin is set to 60mm. Stroke length is also called as wear track diameter, it is the offset distance of pin from the center of rotation of the disc. This combination results into the linear velocity of 2.04m/s and the total distance traveled by the pin is 3675m. The pin is loaded using a dead weight lever arm and the pin holder is heated using a resistance heater for the heating pin and the temperature monitoring is done using a thermostat. The pin holder, in this case, is designed to prevent heat loss from the pin by preventing conduction of heat to lever arm. When the required temperature for running the experiment has reached, the set up is put to hold for 10 minutes before running the machine for complete homogenization. The experiment is performed in accordance with ASTM G99/95a[20]. As the experiment proceeds the reduction in height of the material per second due to wear loss is recorded by a linear variable differential

transformer (LVDT) attached at one end of the lever arm. Friction force exerted on the pin by the disc is recorded using a piezoelectric sensor. Once the experiment is over the set up is allowed to cool for 30 minutes and the surface of the disc is cleaned and polished with a 2500 grit size emery paper. The pin surface having wear tracks is sectioned upto 2mm depth for further characterization as shown in Figure 3.5a.

3.5 Wear track characterization

All the characterization is conducted on the samples tested at the fixed load of 25N at 300K and 573K.

3.5.1 Characterization of samples using SEM

Samples are ultrasonically cleaned with ethanol and then with distilled water for 5 minutes before characterization via FE-SEM. Secondary electron scanning mode at 5KV electron beam with the same procedure as mentioned in section 3.3.2 is used. This mode provides the topological features of the wear track.

3.5.2 Profilometry analysis of the worn surfaces

Two types of profilometers are used here, optical and contact type of profilometer. Three-dimensional surface features and topography of the wear profiles are obtained using optical profilometer of Veeco NT9080 make. It is a non-contact type profilometer where the principle of optical interference and phase shifting is used to scan and quantify topographical features. The profilometer is used in Vertical scanning interferometry (VSI) mode with the array size of 640 x 480 pixels. The contrast between the fringes gives the difference between the peaks.

Contact type stylus profilometer of MarSurf LD130 make is also used to study the topological features of the wear profile over a 2 x 2mm area of the specimen. The stylus having ball radius 2 μ m scans over the surface and the corresponding values of peaks and valleys are reported. Both kinds of profilometers give surface roughness values but the contact ones are sensitive to topographic features and provide accurate estimates.

3.5.3 Characterization through XRD (X-ray diffraction)

X-ray diffraction analysis is carried out on powder XRD machine of Rigaku SmartLab make. The diffractions spectra are obtained by scanning the surface of the samples between 20 to 80 $^{\circ}$ angles. Intensity is plotted against the 2θ , where θ is the

Bragg angle. XRD spectra give a useful information about the type and nature of phases on the sample surface.

3.6 Subsurface microstructure characterization using an optical microscope

The wear samples which are in the form of a disc of diameter 8mm and thickness of approximately 2 mm are further sectioned along the diameter using wire EDM as shown in Figure 3.5. This is followed by etching, metallographic sample preparation and optical microscopy is performed using the procedures described in section 3.3.1 and 3.3.2

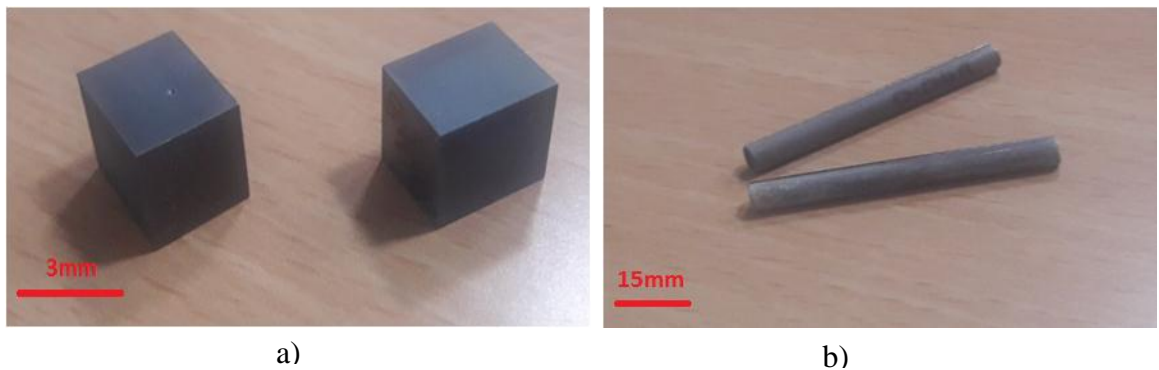


Figure 3.1Specimens used for hardness and wear experiments (a) Cube of edge length 3mm (b) cylindrical pins of diameter 8mm and length of 20 mm

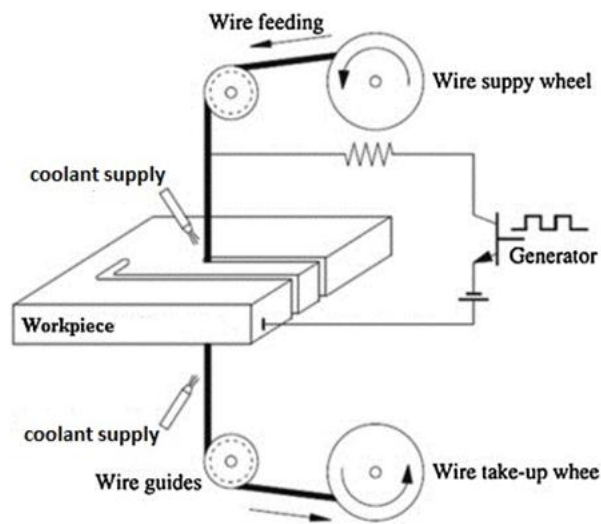


Figure 3.2 Schematic representing the working principle of wire EDM[21]

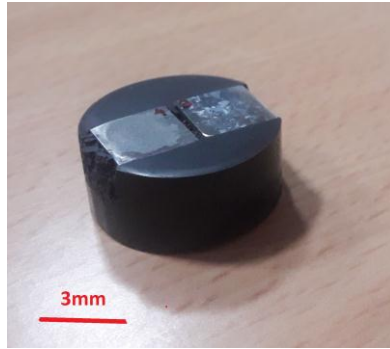


Figure 3.3 Macroscopic image of the hot mounting specimen used for metallographic examination

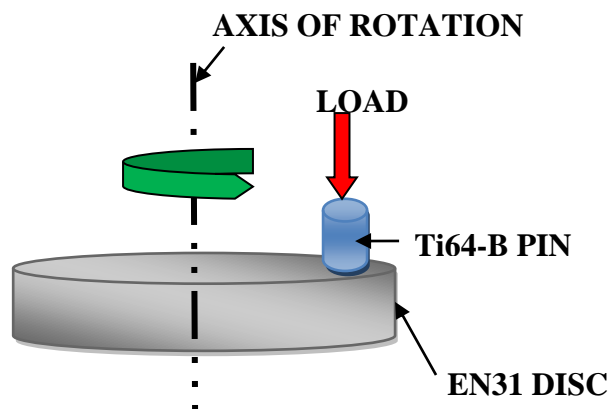


Figure 3.4 Schematic representing the working principle of pin on disc tribometer

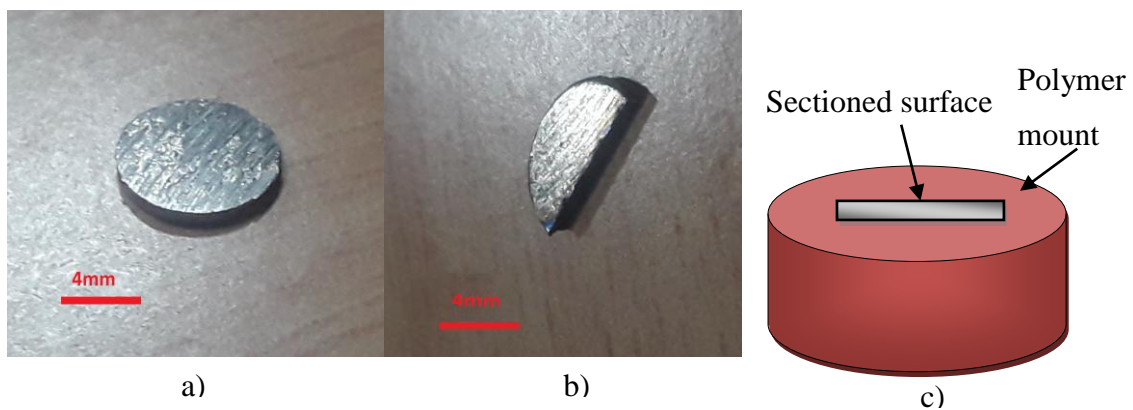


Figure 3.5 (a) Macroscopic optical images of the wear surface of cylindrical pin (b) Sample section for sub-surface microstructural examination (c) mounting of sectioned surface

4 Results

In this chapter, we present the results of wear experiments and corresponding microstructural and topographical analysis of all the three different alloys used in the study.

4.1 Microstructure

The initial microstructure of three different Ti64-B alloys is shown in Figure 4.1 SEM images show lamellar microstructure of Ti64 alloys having alternate α and β laths distributed in prior β grain boundaries. The α lathes are thicker in shape and have dark gray appearance while the β lathes appear light gray. The grain boundary comprises α lathes. The perpendicular α laths when intersecting each other appears like a basket weave structure. TiB particles are elongated whisker-shaped particles of size 2-5 μ m having the dark gray appearance (in 0.3B and 0.55B samples). TiB particles are mostly present around grain boundaries and when their volume fraction increases (like in 0.55B) they form a complete necklace type of structure around grain boundaries. Mainly prior β grain boundaries are decorated with TiB particles. It can be seen from the figure that on subsequent addition of B results into formation of more TiB particles that decorate the grain boundary as well as a reduction in lath size, colony size and grain size is observed. The grain size and colony size is reduced by $\approx 95.8\%$ and $\approx 91.4\%$ respectively with an addition of 0.3wt % of B, then there is a further reduction of $\approx 17\%$ grain size when B content increases from 0.3B to 0.55B. Significant reduction in an aspect ratio of laths can be clearly seen in the microstructural view.[13]

4.2 Pin on disc wear test

Results obtained from pin-on-disc tribometer experiments gives data of height loss i.e. wear, w in microns vs time, t in seconds. Variation of wear loss with time is non-linear initially, as shown in Figure 4.2. As the experiment progresses the variation becomes linear and this transition in time is known as break off period. This could be due to geometric irregularities of the pin surface which results in uneven wear of the pin due to the incomplete contact of a cross-section of the pin with the disc surface. As the wear progresses, complete contact is established between the pin and disc surfaces resulting in a uniform wear of the pin leading to a linear relationship between wear loss and time. To make a better comparison among the samples of different

combination of load, temperature and composition, the wear rate, η is calculated and plotted against the time. The η is defined as the volume of material lost per unit distance traveled by the pin whose units are mm^3/m . Although, the experiments have been conducted from 5 - 25 N with an interval of 5N, the results for 5-15 N are not presented, as the wear rate is not significant at these loads due to low contact pressures. Hence these results are presented only for higher loads (25N). Another set of results obtained from this machine is frictional force vs distance travelled. By dividing frictional force by contact force on the surface we get coefficient of friction (COF) values. Graph of COF vs distance travelled by pin initially increases and the decreases after travelling some distance and finally becomes steady, this steady value is the actual value of COF. (Figure 4.3)

Two types of graphs are plotted here, first is η vs T (at 25N) at different temperatures and the second is η vs B content at 25N for different temperature for pin heating experiments seen in Figure 4.4 and Figure 4.5. It is evident from the figures that the variation of η with temperature is not linear. This indicates that each temperature range different phenomenon for wear is taking place. There is a transition in behavior at approximately 473K where η appears almost steady. For all the compositions the rate of change of wear rate i.e, $d\eta/dT$ at temperature 373K to 473K is reduced by approximately 58% with respect to the rate of change of wear rate at temperature 300K to 373K. Also, there is again a rise of 160% in the rate of change of wear rate at temperature 473K to 573K with respect to the rate of change of wear rate at temperature 373K to 473K. Graphs indicate a very low wear rate for 0.3B than for 0.55B at all temperature. At 373K the difference in wear rate between 0.3B and 0.55B is less than that at 573K. For pure Ti64 the wear rate drastically increases at 573K.

Variation of COF with temperature is plotted in Figure 4.6. It shows that COF increases with temperature which corroborates with an increase in η with T. The differences in COF at high temperatures among the three alloys are negligible while a discernable difference in COF is present at 300 K.

4.3 SEM analysis of wear morphology

SEM analysis is performed on the worn-out surfaces as it provides insight into the underlying macroscopic deformation mechanisms during wear and representative SEM images of worn surfaces are shown in Figure 4.7. At room temperature for all

samples regularly spaced grooves due to abrasive wear can be observed and with increasing the B content these grooves appear more closely spaced. In 0.3B some traces of adhesion wear can be seen. There is more material removal via abrasion wear at a higher temperature for pure Ti64 with deeper grooves. For 0.3B and 0.55B at a highertemperature, there is more delamination wear which is more severe in 0.55B samples. The plowing and delamination features are indications of abrasive and delamination wear.

4.4 Profilometer analysis of wear tracks

Contact Profilometer analysis of pin heating samples (Figure 4.8) indicate the reduction in asperities spacing with an increase in Boron content (which can be clearly seen in SEM images as well) as well as with temperature increase. There is an increase in average roughness value (Ra) with Boron content. But for boron modified alloys there is a reduction in average roughness value at high temperature.

4.5 XRD analysis of wear tracks

The diffraction spectra of worn-out surfaces are shown in Figure 4.9 with the intensity plotted on the abscissa and 2θ on the ordinate where θ is the Bragg angle. The intensity peaks and their positions are matched with the standard crystallographic data, this clearly shows the presence of α -Ti, β -Ti and TiB suggesting that no tribo-oxides are formed on the surface of the samples at all temperature. For 0.55B alloy in particular at 300 K the presence of TiB peaks are observed which is not observed either in TiB at 573 K or all other samples.

4.6 Subsurface microstructure analysis:

The optical microscope images of the subsurface of wear tracks are shown in Figure 4.10. The kinking of laths at room temperature is observed for all the samples. Higher the B content, lower is the aspect ratio of the laths and lower is the kinking. The maximum kinking angle for 0.0B is approximately 98° , for 0.3B it is 80° and for 0.55B is 50° . At higher temperature for all samples kinking is not observed or may be negligible with a comparison to room temperature samples.

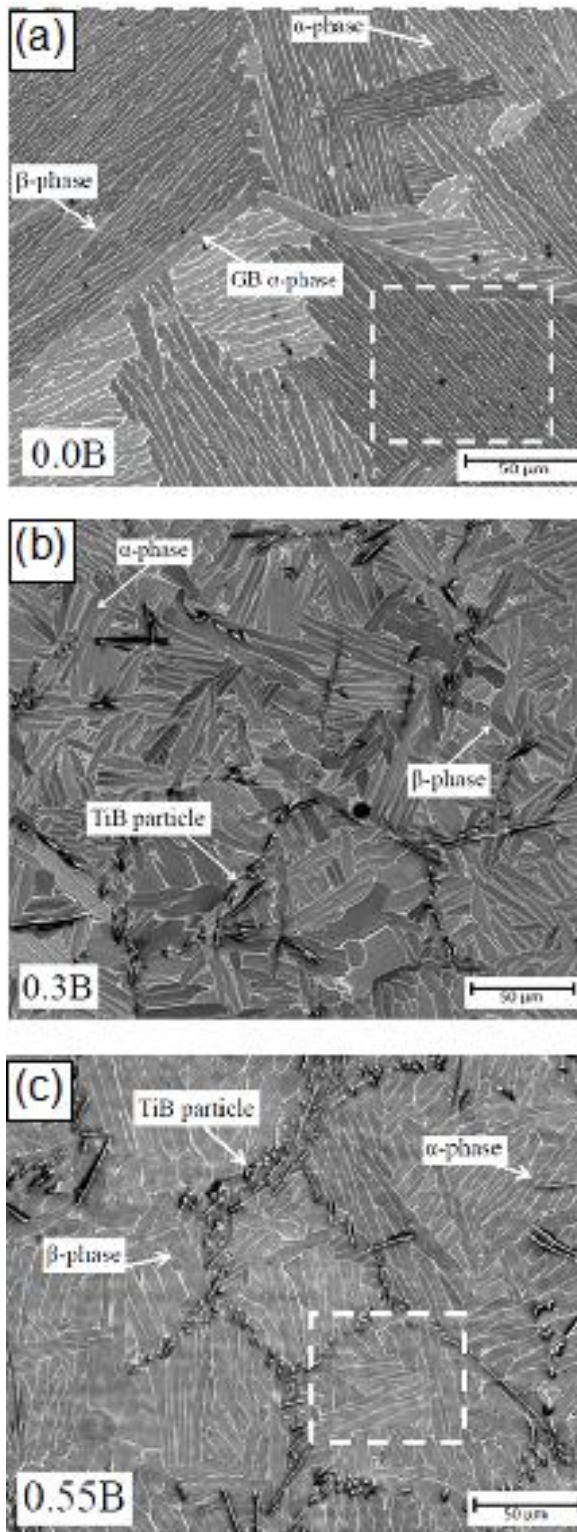


Figure 4.1 Scanning electron microscopy images of microstructures of Boron modified Ti64 alloys with (a) 0.0B (b) 0.3B and (c) 0.55B

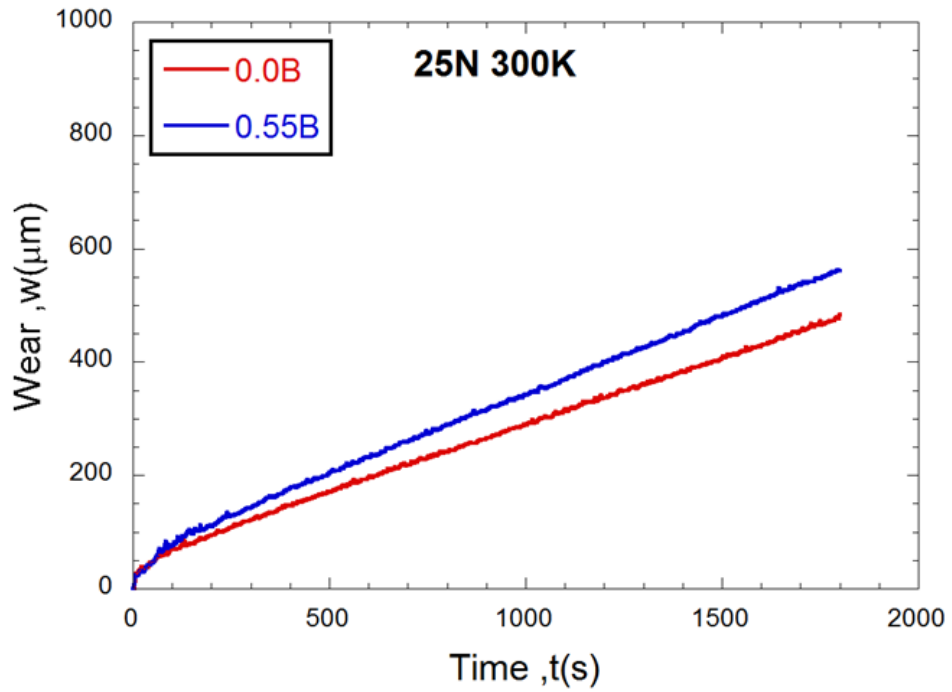


Figure 4.2 Variation of wear, w with time, t obtained from Pin-on-disc tribometer

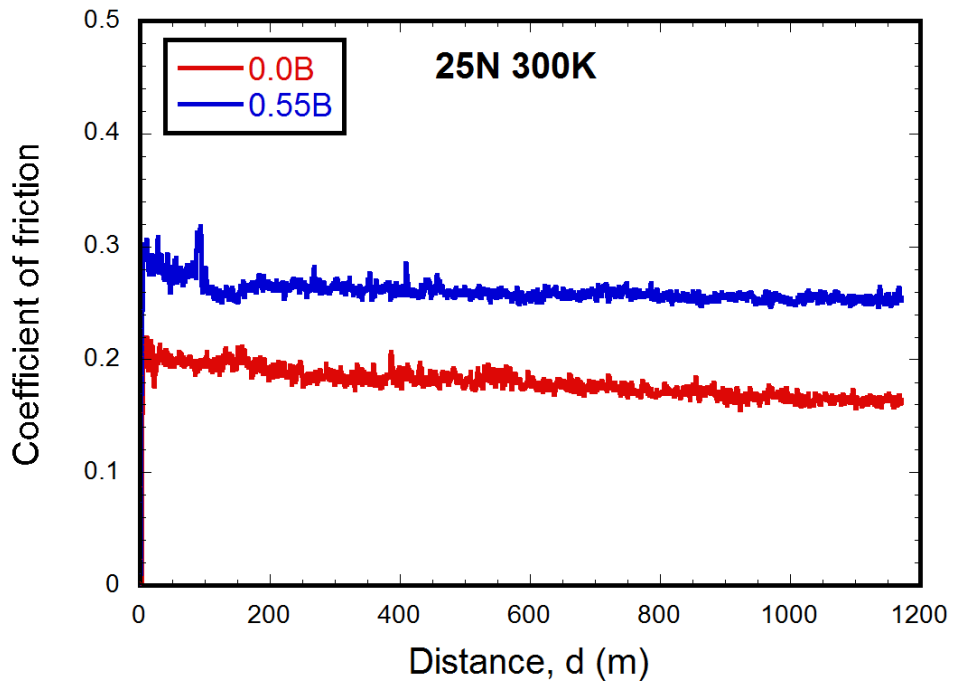


Figure 4.3 COF plotted against the sliding distance at a normal load of 25N

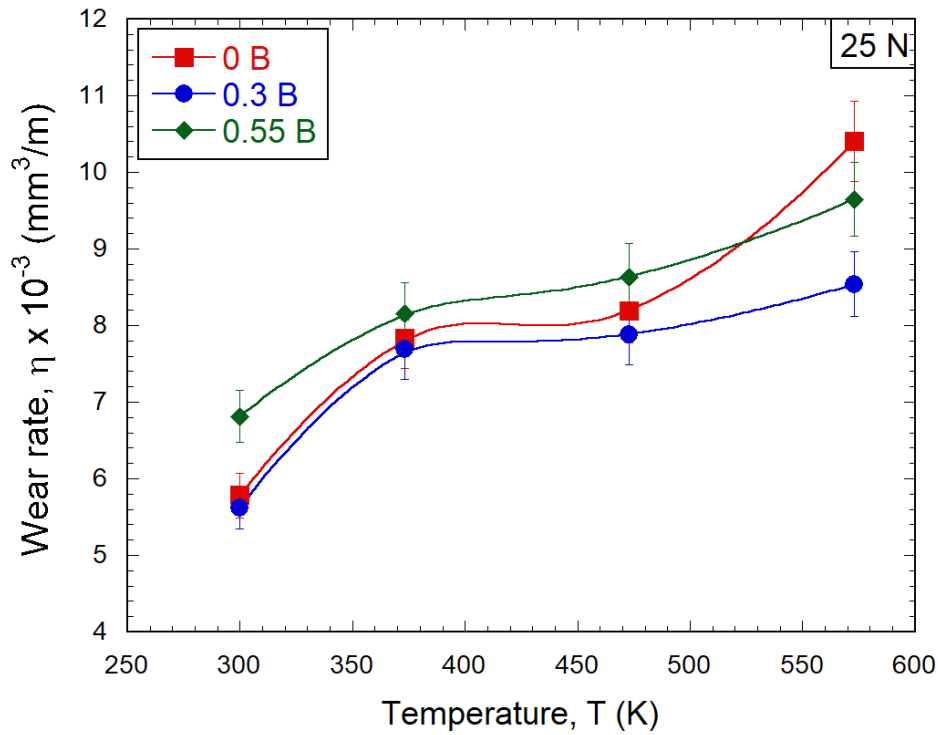


Figure 4.4 Variation of wear rate, η with temperature at 25N load for the three different Ti64-B alloys

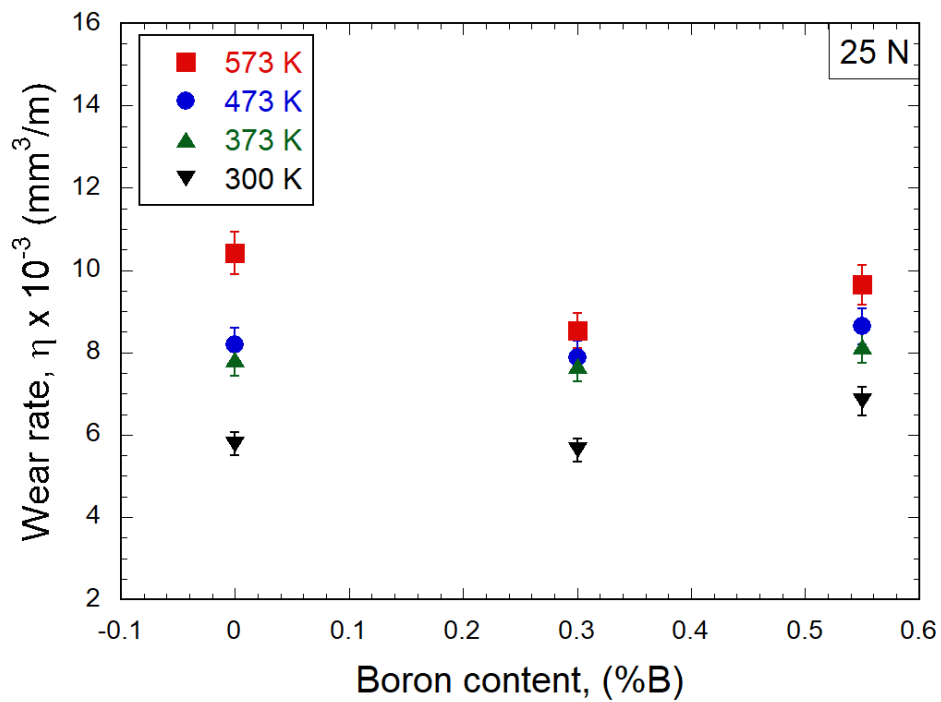


Figure 4.5 Variation of wear rate η with Boron content at 25N load at different temperatures.

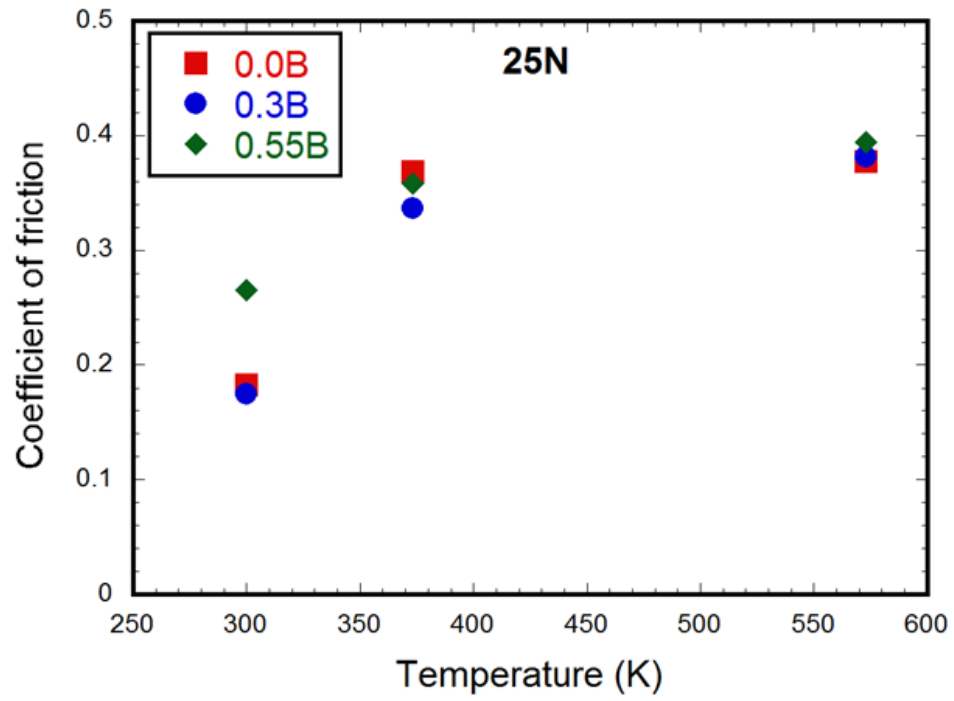
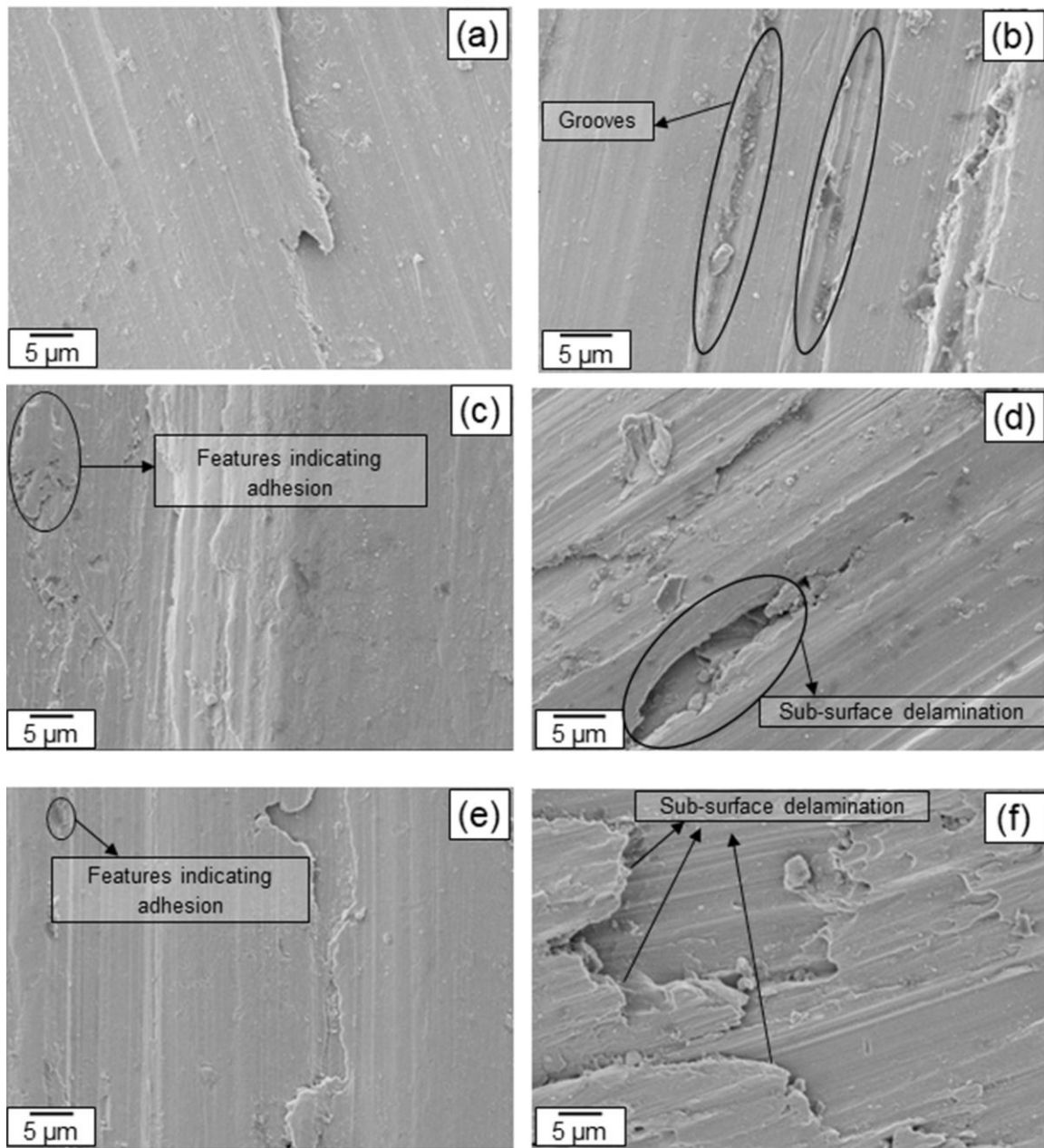


Figure 4.6 Representative plot showing the variation of COF with temperature at a constant load of 25N for all three alloys



Figure

Figure 4.7 SEM images of wear surfaces of Ti64 alloys tested at 25N under various combinations of temperature and composition of (a) 300 K, 0 B (b) 573 K, 0 B (c) 300 K, 0.3 B (d) 573 K, 0.3 B (e) 300 K, 0.55 B (f) 573 K, 0.55 B

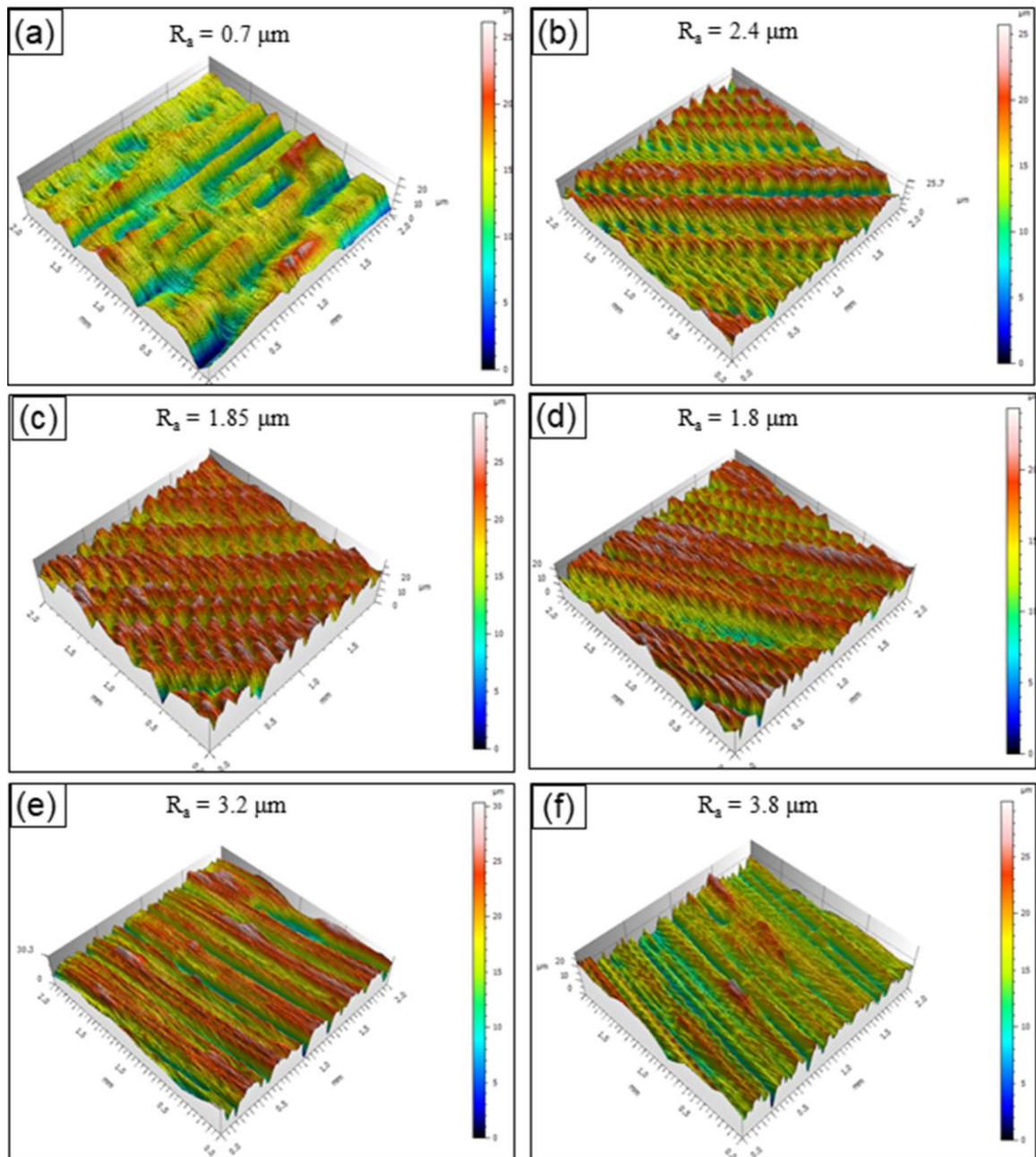


Figure 4.8 Contact profilometer images of the worn-out surfaces of Ti64 alloys tested at 25 N for composition and temperature of (a) 0B, 300 K (b) 0 B, 573 K (c) 0.3B, 300 K, (d) 0.3 B, 573 K (e) 0.55 B, 373 K (f) 0.55 B, 573 K

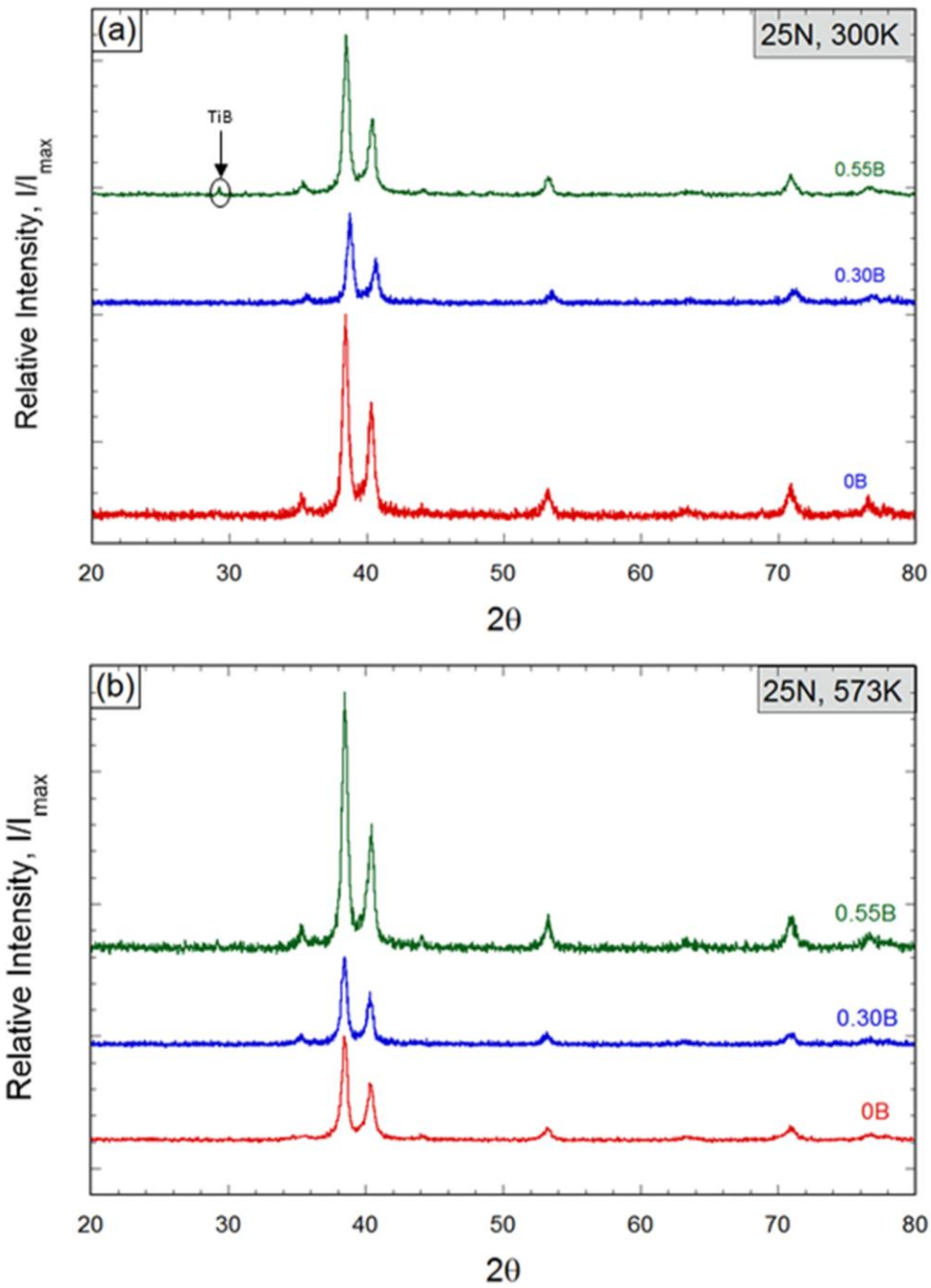


Figure 4.9 XRD patterns obtained on the wear surfaces of Ti64-B samples subjected to wear testing at (a) 300 K and (b) 573 K.

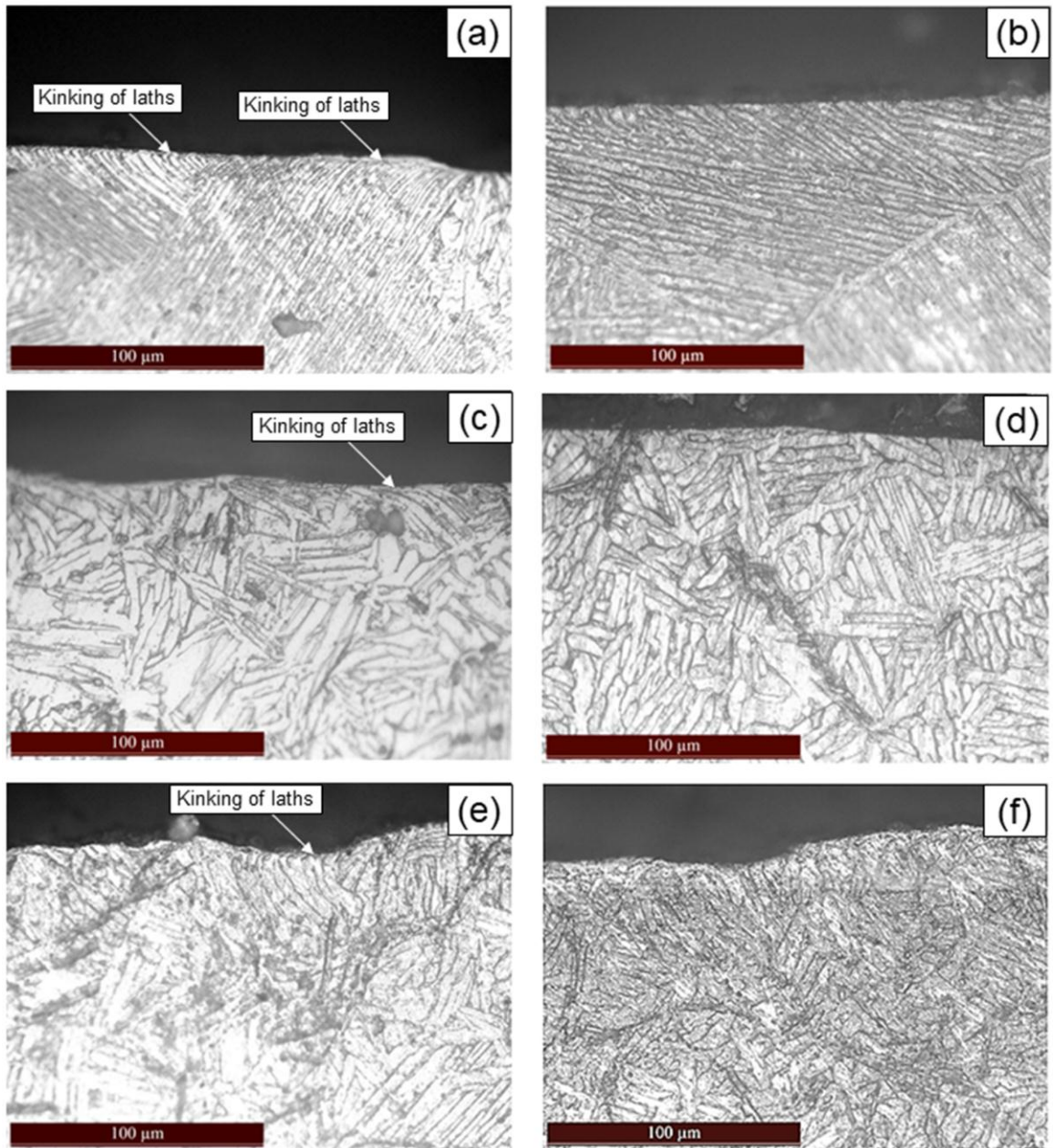


Figure 4.10 Cross sectional optical micrographs of sub-surface regions just below the wear surface of Ti64 alloys tested at 25 N under (a) 0B, 300 K (b) 0 B, 573 K (c) 0.3B, 300 K, (d) 0.3 B, 573 K (e) 0.55 B, 300 K (f) 0.55 B, 573 K

5 Discussion

In this chapter, the critical analysis and justification of the results will be presented.

5.1 Analysis of results of the pin on disc experiments

The coefficient of friction (COF) *vs* distance (Figure 4.2) curves shows extensive serrations, oscillation about a mean line as the distance covered increases. During the initial state, there is strong interaction between the asperities between the pin and disc surface resulting in an increase in friction force and the COF values during this state are more or less equal to static friction value. After this stage, the asperities get flattened, and the two surfaces starting slipping against each other as a consequence the COF decreases. In this stage, there is a change in the COF from static to kinetic friction. Another feature that should be observed in the abrupt increase in COF in the initial state in Figure 4.2 can be explained based on the geometric argument. In this stage, the pin and disc surface do not form confirming contact as the pin surface may not be completely flat with respect to the disc surface. A slight misalignment in the sample also could be lead to this behavior. This also explains the initial non-linear behavior of the wear, *w vs* time plot (Figure 4.1).

COF depends on the following factors:

- Hardness- as the hardness increases the COF decreases; this is due to nonadherence of the hard material to its mating material.
- Elasticity modulus *E*- increase in *E* decreases adhesion and COF.
- Grain size- on decreasing the grain size COF decreases due to improved hardness.
- Temperature- higher the temperature more is the susceptibility to oxide layer formation which reduces COF due to its lubricating effect. At higher temperature, there is also the chance of material softening due to dynamic globulization which can increase COF.
- Normal load- oxide films reduce COF and increase in normal load breaks this oxide layer. Therefore there is an increase in COF.
- Sliding velocity- high-velocity results at high temperature due to frictional heating and either result in the formation of the oxide layer that reduces COF or into thermal softening which increases COF.

The COF obtained in our results as shown in Figure 4.6 is due to the cumulative effect of all these factors.

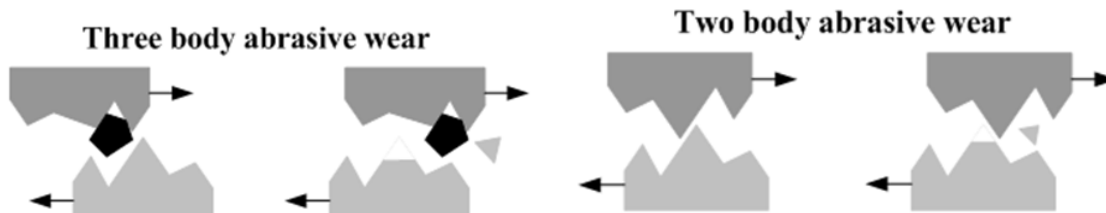
The wear loss is governed by the mechanisms taking place at the pin-disc interface. These mechanisms are typically governed by the mechanical and physical properties of the pin and disc material, the microstructure of the materials and the external parameters used in the wear test. The materials experience multiple wear mechanisms at different stages of wear. A brief description of different types of wear mechanisms experienced by the samples during the wear test are explained below along with their cartoons, (Figure 5.1) representing the way in which material loss happens during these mechanisms.

- ❖ Adhesive wear- This mechanism is primarily noticed during the initial stages of wear, at low normal loads, very high temperatures and when the relative differences in hardness values between the pin and disc material is less. During the adhesive wear, strong Van der Waal forces present at the vicinity of topological features of the material creates adhesive bonding between the mating parts. Due to the relative motion between the two materials the softer material gets sheared and sticks to harder material, subsequently, in the sliding phase, this adhered material gets removed in form of debris.[22]
- ❖ Abrasion wear- This mechanism is active typically under high loads, later stages of the wear where sufficient hardening of the softer material has taken place. During the abrasive wear, the asperities of hard material plow over the surface of soft material resulting in the formation of grooves. This is classified into two types: two bodies and three body abrasion. In two-body abrasion, the material removal is only due to abrasive actions of pin and disc. In three body abrasion wear, wear debris, formed due to the rubbing action between the two mating parts, also participate in the wear process. The wear debris typically includes hard second phase particles or foreign inclusions which aggravate the wear rate by plowing and cutting mechanism.
- ❖ Delamination wear- according to Suh [23] at large plastic strains, there is a net difference in the dislocation densities between the surface and sub-surface regions of the sample. This is mainly due to large image forces experienced by the dislocations which are closer to the surface than the interior ones. The differences in dislocation densities will lead to large plastic deformation

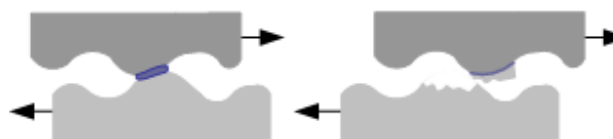
gradients between two regions of the sample. This often causes a nucleation of voids, subsurface cracks which grow and coalesce as the deformation progress, eventually resulting removal of the material in the form of thick sheets and laminates.

❖ Oxidation wear- This wear mechanism is noticed in the case of highly reactive metals (e.g. Al, Ti) and the oxide layer plays a major role in controlling the wear. Since metals oxides typically are high melting materials with very high hardness, the presence of lubricating oxide layer decreases the wear rate. In addition to the microstructures, the ambient conditions have a major role in governing the oxidation wear. In general, high temperatures promote the oxidation and the Pilling–Bedworth ratio determines the mechanical stability of the oxide layer. At low to intermediate loads, the oxide layers are stable so there is less wear of the material, while at high load, the frictional forces are high enough to drive off the oxide layers from the pin surface which increases the wear rate.

Abrasive wear



Adhesive wear



Delamination wear

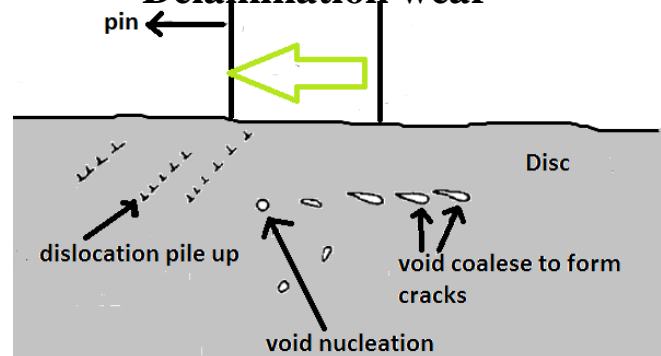


Figure 5.1 Prominent types of wear mechanisms [24]

Factors affecting the wear rate:

- Normal load- increasing normal load increases wear rate due to more contact stresses which causes more plastic deformation resulting into more material removal. The high load can also cause the removal of the lubricating oxide film, therefore, results in more material removal.
- Sliding velocity- as sliding velocity increases the frictional heat increases and there is more tendency for tribo oxides formation. In turn, these tribo oxides act as lubricants against wear.
- Temperature- apart from oxide formation higher temperature can also cause material softening resulting into more wear if the counter material retains its hardness.
- Hardness- according to Archard's model wear rate is inversely proportional to hardness since there is lesser plowing due to more hardness, therefore, less wear rate in case of abrasive wear.
- Elastic modulus E- higher the value of E lesser is the wear resistance in case of abrasive wear. While in case of adhesive wear high elastic modulus means low adhesion to the hard material surface.
- Fracture toughness- in case of moderate to severe wear where the crack nucleation governs the wear phenomenon, fracture toughness plays an important role. When fracture toughness is the high propensity of crack growth is less and therefore more wear resistance.

Table 5-1 Table explaining the effect of B on properties and factors/ properties that govern wear rate and COF

Factors/ properties affecting wear rate	Effect of increasing B content on properties	Effect on COF	Effect on wear rate
Hardness	increases	Decreases	decreases
Elasticity modulus	increases	Decreases	decreases
Sliding velocity	NA	Increase/decrease	Increase/decrease
Fracture toughness	decreases	NA	increases

Temperature	NA	Increase/decrease	Decreases/increases
Normal load	NA	increases	increases

According to research conducted by Budinski [25], abrasive wear of Ti64 alloys is more than commercially pure Ti although Ti64 is much harder, this result is contradictory to Archard's law which states that abrasion resistance is inversely proportional to the hardness of alloy. The reason behind this is the $\alpha+\beta$ microstructure of Ti64 alloys which has a surface pattern like a tire with treads. When the rolling abrasive particles come under its surface they tend to momentarily stick in these tread like region and causes wear of material in those regions. While in case of commercially pure Ti (which has only one phase), the abrasive particles roll away from the pin disc interfaces and do not participate in the wear. Molinari *et. al* [26] reported that the main reason behind low wear resistance of Ti alloys is lack of work hardening as they exhibit a elastic-perfectly plastic behavior. Further, TiO forms a weak oxide layer and does not remain adhered to the Ti alloy surface.

It is evident from the results that η increases with increasing load and this is due to the increase in contact pressure between the two mating surfaces. A similar trend has been reported in the literature during the dry sliding wear of wrought Ti64 alloys [27–29]

There have been experimental investigations highlighting the role of grain size on the wear behavior. Mishra *et al.* [30] and Farhat *et al.*[31] have carried out experiments on Ni and Al with varying grain sizes and found a higher wear resistance for nanocrystalline materials which is attributed to the decrease in coefficient of friction due to the decrease in grain size. A similar trend has been noticed by Breglio *et al.* [32] during the wear testing of austenitic stainless steel. Therefore, both the decrease in grain and lath sizes should lead to an increase in wear resistance of the Ti64 alloys and in such case both 0.3 B and 0.55 B alloys should show a higher wear resistance compared to B free Ti64 alloys. However, the current observations (Figure 4.4) indicate a lower wear resistance of 0.55 B alloy than the Ti64 alloys containing 0 B and 0.3 B. Among the three alloys, the alloys with 0.3 B shows the best wear resistance, i.e. the wear resistance increases, initially with B content and decrease

thereafter. The reasons for this anomalous behavior will be discussed in the subsequent sub-sections.

5.2 Morphologies of the worn-out surfaces

The representative morphologies of the worn-out surfaces at room and high temperatures, for the three alloys, are presented in Figure 4.7 and Figure 4.8. Both SEM and profilometry images clearly indicate distinct deformation features at low and high temperatures. It can be noticed from Fig. 4.7 that at room temperature, the samples surfaces show more abrasive wear with an intensive shearing of the material while at high temperature more delamination is observed. The cutting and plowing features are indications of abrasive when hard particles penetrate into the softer matrix thereby creating deeper groves and asperities. In typical metal-metal contact, due to the severe rubbing between the two surfaces, initially, there will be a transfer of material between these surfaces resulting in adhesive wear [22,33–35]. This is observed in Figure 4.7 c. Even the profilometer images and the corresponding surface roughness indicate the distinct deformation features existing between the as-cast and Boron modified alloys. The spacing between the asperities is higher for 0B alloys compared to the 0.3B and 0.55B alloys and which could be attributed to their large grain and lath sizes. It can be also be observed from Figure 4.8 that, the inter-asperity spacing decreases with increasing B content suggesting more shearing of material by abrasive action.

In the case of microstructure containing hard TiB precipitate particles, the coherency between the matrix and precipitate particles govern further wear mechanisms and wear rate. The debonding of TiB precipitates depends on the load, sliding conditions, sliding velocity, and temperature. The debonding of the TiB particles occurs due to the plastic strain in-compatibilities between the matrix and Ti64 matrix, and also due to the high pile-up stresses existing at the interface of the two surfaces. At high temperature due to a significant difference in coefficient of thermal expansion of TiB particles and Ti64 alloys (TiB- $6.4 \times 10^{-6}/K$ and Ti64- $8.6 \times 10^{-6}/K$ at 250°C [36]) thermal stresses generate which again results into more removal of TiB particles[37].The debonding of the particles leads to the formation of surface and sub-surface cracks and these cracks propagate and coalesce into larger cracks often leading to the removal of surface layers in the form of a laminates[23]. Also the three-body wear process often causes the delamination of the subsurface layers resulting in

delamination wear. Therefore the second phase particles (TiB) are often detrimental to wear as they also participate in the wear and accelerate the material removal. The propensity of the delamination wear increases with decreasing fracture toughness of the material and in the case of Boron modified as cast Ti-64 alloys, Sen *et al.* [11,12] have reported that the mode-I fracture toughness, K_{Ic} , decreases with increase in B content. The wear rate doesn't linearly vary with the B content, it decreases initially to 0.3B and subsequent addition of B results in an increase in wear rate Figure 4.4. A similar trend was noticed by Venkatraman and Sundararajan [38,39] in Al-SiC composites in which the wear rate decreases to a volume fraction of 10% SiC and further additions of SiC increases the wear rate. Their analysis suggests that the volume fraction of the SiC particles controls the thickness of the sub-surface deformed layer which in-turn influences the wear mechanisms and wear rate

Further, the XRD analysis of worn surfaces at 573K (Figure 4.9) supports this claim as the peak corresponding to TiB is absent from the surface. The coefficient of friction values was also found to increase with an increase in temperature which is consistent with the increase in wear rate.

5.3 Subsurface microstructures

The optical micrographs of the region just beneath the wear surface are given in Figure 4.10. The subsurface microstructures reveal distinct deformation features at room and high temperatures. Severe kinking of the laths is noticed at room temperature (Figs. 4.10 a,c and e) and such features are observed even during the wear of wrought Ti alloys [27]. The reasons for lath kinking at room temperature is the high shear stresses acting at the pin-disk interface. This is a dominant mechanism by which material loss occurs from the pin during wear. While at high temperatures, where diffusion related phenomena are very active and kinking of laths is not significant. It is seen that as the lath size increases the kinking angle increases i.e. the material can sustain more shear stresses. Since lath size is maximum in 0B it will have least abrasion wear and this result corresponds to SEM images of wear surface as well. Another important observation from the Fig. 4.10 is the waviness associated with the 0.55 B alloy compared to 0 and 0.3B alloys when viewed along the cross-section. This has also been supported by the severe oscillations noticed in the profilometer images of 0.55 B and high average roughness (Ra) associated with the worn surface.

5.4 Formation of surface oxides and their influence on the wear behavior

Pauschitz in his research [35] paper described the 3 types of tribo layers:

1. The first type is known as a transfer layer, this is formed at low temperature (so lower oxidation) and is formed when both sliding materials are of the same type. This layer is usually weak.
2. This layer is known as a mechanically mixed layer (MML) and it is formed at a high temperature with more oxide formation. Here the sliding material is comparatively hard.
3. A composite layer which is formed at a higher temperature with more oxygen content, it is very hard and brittle.

Zhang *et al.*[40] have found that under ambient conditions, certain combinations of the load and temperatures lead to the formation of tribo-oxides and their participation in the wear process depends on the contact pressure between the pin and disc. At intermediate loads and high temperatures, the tribo-oxides participate actively in the wear process and because of their increased hardness, they increase the wear resistance of the material. However, at very high loads, the high contact pressures breaks down the protective tribo-oxide layers and thus resulting in an increase in wear rate. As the temperature increases the amount of oxides increases which increases the hardness of this layer, therefore the hardness of tribo layer is very low at room temperature. Mao *et al.* [29] also found that oxidation is the major factor that controls the formation of MML and thus influences the wear properties.

X.X.Li and coworkers [27,41] reported that on increasing sliding velocity at a fixed load and temperature, the wear rate increases reaching a maximum and then decreases. At lower speed there was metallic plus oxidative wear, at intermediate speed there was only metallic wear and at the high speed, there was only oxidation wear. Formation of ceramic type mechanically mixed layers (MML) is reported. There is a balance between 2 processes one is formation of tribo oxides due to more heat generation as the velocity is increased and other is the removal of tribo oxides from the surface as they are formed due to centrifugal force. At the intermediate speed where the wear rate is maximum, there is no presence of tribo oxides and MML. X.X.Li also reported that MML is formed during pre sliding sample at high speed and

it further prevents wear when the material was sliding at lower speed having more wear rate at normal conditions.

There were some researchers who reported that oxide formation did not help in wear resistance and in fact they increased the wear rate. Molinari *et al.* [26] reported that Ti oxides are very weak, loose and brittle and initially they are the major factors contributing to the increased wear rate, so overall they provide no protection towards wear unlike in case of other metals and their alloys. In a research by Farokhzadeh [28], it was reported that the failure of MML occurs by microcrack formation below MML layer.

In our experiments, the formation of tribo-oxides on the wear surface might have influenced the wear performance.

The X-ray diffraction spectra of the worn surfaces at a load of 25N and under the test temperatures of 300 and 573 K are shown in Figure 4.9 clearly shows the absence of surface oxides on the worn surface. This indicates that the observed wear response is completely due to the pin-disc material eliminating the role of an intermediate oxide layer. Also, COF would have decreased if there was the presence of tribo oxides since they act as lubricants. It can be concluded from these results that the formation of oxides at a normal load of 25 N, for the combination of cast Ti64-B and steel tribo pair, requires much higher temperatures.

6 Conclusion and future scope

Microstructures containing more TiB particles show more wear especially at high temperature. With increase in B content the wear rate decreases up to 0.3B and then increases up to 0.55B. Overall alloys having 0.55B wt. % Boron shows better mechanical properties than 0.3B but on contrary shows lower wear properties.

Observed dominant mechanism of wear are of two types abrasion and delamination wear. Abrasion wear is more dominant at lower temperature and boron content while delamination wear is more dominant at higher temperatures and higher B content.

Since Ti64 alloys is used in contact loading conditions with harder alloys like EN31, research should be further carried out at different conditions of velocity, humidity, surface heating, etc

REFERENCES

- [1] G. Lütjering, J.C. Williams, Titanium, 2nd ed., Springer, Berlin, 2007.
- [2] T.Choda, H. Oyama, S. Murakami, Technologies for Process Design of Titanium Alloy Forging for Aircraft Parts, Kobelco Technology. (2015).
- [3] J. Zhu, A. Kamiya, T. Yamada, W. Shi, K. Naganuma, Influence of boron addition on microstructure and mechanical properties of dental cast titanium alloys, Mater. Sci. Eng. A. 339 (2003) 53–62.
- [4] S. Tamirisakandala, D. B. Miracle, Microstructure engineering of titanium alloys via small boron additions, Int. J. Adv. Eng. Sci. Appl. Math. 2(4) (2010) 168–180.
- [5] www.superaalloys.com.
- [6] www.upmet.com.
- [7] www.dierk-raabe.com.
- [8] K.S. Ravichandran, K.B. Panda, Titanium composited with TiB whiskers, Advanced Materials, and Processes. (2002).
- [9] www.aerospacemetals.com.
- [10] I. Sen, S. Tamirisakandala, D.B. Miracle, U. Ramamurty, Microstructural effects on the mechanical behavior of B-modified Ti–6Al–4V alloys, Acta Mater. 55 (2007) 4983–4993.
- [11] R. O. Ritchie, J. F. Knott, J. R. Rice, On the relationship between critical tensile stress and fracture toughness in mild steel, J. Mech. Phys. Sol. 21 (1973) 395–410.
- [12] I. Sen, K. Gopinath, R. Datta, U. Ramamurty, Fatigue in Ti–6Al–4V–B alloys, Acta Mater. 58 (2010) 6799–6809.
- [13] I. Sen, U. Ramamurty, Elastic modulus of Ti–6Al–4V–xB alloys with B up to 0.55 wt.%, Scr. Mater. 62 (2010) 37–40.

- [14] P. Agrawal, S. Karthikeyan, Enhancement in Strain Hardening on Boron Addition in As-Cast Ti–6Al–4V Alloy, *Trans. Ind. Inst. Met.* 68 (2015) 195–205.
- [15] G. Singh, I. Sen, K. Gopinath, U. Ramamurty, Influence of minor addition of boron on tensile and fatigue properties of wrought Ti–6Al–4V alloy, *Mater. Sci. Eng. A.* 540 (2012) 142–151.
- [16] G. Singh, D. V. V. Satyanarayana, R. Pederson, R. Datta, U. Ramamurty, Enhancement in creep resistance of Ti–6Al–4V alloy due to boron addition, *Mater. Sci. Eng. A.* 597 (2014) 194–203.
- [17] I. Sen, R. S. Kottada, U. Ramamurty, High-temperature deformation processing maps for boron modified Ti–6Al–4V alloys, *Mater. Sci. Eng.*, 527 (2010) 6157–6165.
- [18] I. Sen, G. Karthikeyan, J. Ramkumar, R. Balasubramaniam, A Study on Machinability of B-Modified Ti-6Al-4V Alloys by EDM, *Mat. Manuf. Proc.* 27 (2012) 348–354.
- [19] S. Kuriakose, M.S. Shunmugam, Characteristics of wire-electro discharge machined Ti6Al4V surface, *Mater. Lett.* 58 (2004) 2231–2237.
- [20] ASTM G 99 – 95a Standard Test Method for Wear Testing with a Pin-on-Disk Apparatus1, (2000).
- [21] R. K. Fard, R. A. Afza, R. Teimouri, Experimental investigation, intelligent modeling and multi-characteristics optimization of the dry WEDM process of Al-SiC metal matrix composite, *Journal of Manufacturing Processes.* 15 (2013) 483–494.
- [22] P. L. Menezes, S. P. Ingole, M. Nosonovsky, S. V. Kailas, Michael R. Lovell, *Tribology for Scientists and Engineers*, 1st ed., Springer, New York, 2013.
- [23] N. P. Suh, The delamination theory of wear, *Wear.* 25 (1973) 111–124.
- [24] www.subtech.com.
- [25] K. G. Budinski, Tribological properties of titanium alloys, *Wear.* 151 (1991) 203-217.

- [26] A. Molinari, G. Straffelini, B. Tesi, T. Bacci, Dry sliding wear mechanisms of the Ti6Al4V alloy, *Wear*. 208 (1997) 105–112.
- [27] X.X. Li, Q. Y. Zhang, Y. Zhou, J. Q. Liu, K. M. Chen, S. Q. Wang, Mild and Severe Wear of Titanium Alloys, *Tribol. Lett.* 61 (2016) 14–22.
- [28] K. Farokhzadeh, A. Edrissy, Transition between mild and severe wear in titanium alloys, *Trib. Int.* 94 (2016) 98–111.
- [29] Y. S. Mao, L. Wang, K. M. Chen, S. Q. Wang, X. H. Cui, Tribo-layer and its role in dry sliding wear of Ti–6Al–4V alloy, *Wear*. 297 (2013).
- [30] R. Mishra, B. Basu, R. Balasubramaniam, Effect of grain size on the tribological behavior of nanocrystalline nickel, *Mater. Sci. Eng., A*. 373 (2004) 370–373.
- [31] Z.N. Farhat, Y. Ding, D.O. Northwood, A. T. Alpas, Effect of grain size on friction and wear of nanocrystalline aluminum, *Mater. Sci. Eng., A*. A206 (1996) 302–313.
- [32] G. Bregliozzi, A. Di Schino, J. M. Kenny, H. Haefke, The influence of atmospheric humidity and grain size on the friction and wear of AISI 304 austenitic stainless steel, *Mater. Lett.* 57 (2003) 4505–4508.
- [33] H. Kato, Effects of supply of fine oxide particles onto rubbing steel surfaces on severe–mild wear transition and oxide film formation, *Trib. Int.* 41 (2008) 735–742.
- [34] F.H. Stott, High-temperature sliding wear of metals, *Trib. Int.* 35 (2002) 489–495.
- [35] A. Pauschitz, Manish Roy, F. Franek, Mechanisms of sliding wear of metals and alloys at elevated temperatures, *Tribol Int.* 41 (2008) 584–602.
- [36] *Material Properties of Titanium Diboride*, (2000).
- [37] R. J. Arsenault, N. Shi, Dislocation Generation Due to Differences between the Coefficients of Thermal Expansion, *Materials Science, and Engineering A*. 81 (1986) 175–187.

- [38] B. Venkataraman, G.Sundararajan, The sliding wear behaviour of Al-SiC particulate composites-I. Macrobehaviour, *Acta Mater.* 44 (1996) 451–460.
- [39] B. Venkataraman, G.Sundararajan, The sliding wear behaviour of Al-SiC particulate composites-II, The characterization of subsurface deformation and correlation with wear behaviour, *Acta Mater.* 44 (1996) 461–473.
- [40] Q. Y. Zhang, Y. Zhou, L. Wang, X. H. Cui, S. Q. Wang, Investigation on tribo-layers and their function of a titanium alloy during dry sliding, *Tribo. Int.* 94 (2016) 541–549.
- [41] X.X. Li, Y.Zhou, X.L.Ji, Y.X.Li, S.Q.Wang, Effects of sliding velocity on tribo-oxides and wear behavior of Ti–6Al–4V alloy, *Tribo. Int.* 91 (2015) 228–234.